Safe Coverage of Compact Domains For Second Order Dynamical Systems

by

Juan David Chacon Leon

B.Eng., Universidad Distrital Francisco José de Caldas, 2017
M.Sc., Universidad Nacional de Colombia, 2016
B.Sc., Universidad Nacional de Colombia, 2014

Thesis Submitted in Partial Fulfillment of the
Requirements for the Degree of
Master of Science

in the
Department of Mathematics
Faculty of Science

SIMON FRASER UNIVERSITY
Summer 2020

Declaration of Committee

Name:	**Juan David Chacon Leon**
Degree:	**Master of Science (Applied and Computational Mathematics)**
Thesis title:	**Safe Coverage of Compact Domains For Second Order Dynamical Systems**
Committee:	**Chair:** Nilima Nigam Professor, Mathematics
	Razvan Fetecau Supervisor Professor, Mathematics
	Mo Chen Committee Member Assistant Professor, Computing Science
	Weiran Sun Examiner Associate Professor, Mathematics

Abstract

Autonomous systems operating in close proximity with each other to cover a specified area has many potential applications, but coordination and safety are two fundamental challenges. For coordination, we propose a locally asymptotically stable distributed coverage controller for moving compact domains for two types of vehicles with second order dynamics (double integrator and fixed-wing aircraft) with bounded input forces. This control policy is based on artificial potentials and consensus forces designed to promote desired vehicle-domain and inter-vehicle separations and relative velocities. We prove that certain coverage configurations are locally asymptotically stable. For safety, we establish minimal energy conditions for collision free motion and we utilize Hamilton-Jacobi (HJ) reachability theory for pairwise collision avoidance. Rather than computing numerical solutions of the associated HJ partial differential equation, we derive an analytical solution for the double integrator vehicle. We demonstrate our approach in several numerical simulations involving convex and non-convex moving domains.

Keywords: Autonomous robots; swarm intelligence; decentralized control; Hamilton-Jacobi reachability; artificial potentials; coverage control.

Dedication

This thesis is dedicated to my lovely partner Lorena, my parents and especially to my brother Daniel, whose desire to overcome has been inspiring.

Acknowledgements

I would like to express my deepest appreciation to my supervisors Razvan Fetecau and Mo Chen for their guidance, dedication and patience during these almost two years of research, working with them was a pleasure. I would like to extend my gratitude to the SFU MARS lab members, especially to Minh Bui, Xubo Lyu, Anjian Li for their support and valuable feedback. This thesis has benefited from the conversation with other graduate students at Simon Fraser. I would like to thank Thomas Retzloff, Kurnia Susvitasari, Negin Karimani and Mohsen Seifi for offering encouragement and advise. I would like to extend my sincere thanks to Christie Carlson and the SFU Mathematics department for their extraordinary support in the hardest times. Last but not least, I am grateful to my friends Juan Garcia, Joey Burgos, Alejandro Silva for supporting my efforts.

Table of Contents

List of Tables

List of Figures

Chapter 1

Introduction

Autonomous systems have great potential to positively impact society. However, these systems still largely operate in controlled environments in the absence of other agents. Autonomous systems cooperating in close proximity with each other has the potential to improve efficiency. Specifically, in this thesis we consider the problem of controlling multiple autonomous systems to cover a desired possibly moving area in a decentralized and safe manner. More precisely, two key challenges need to be addressed: coordination and safety.

In coverage control problems, the objective is to deploy agents within a target area, or domain such that they can achieve an optimal sensing of the domain of interest. A common approach to the coverage problem is by means of Voronoi diagrams ([14, 23]), where the goal is to minimize a coverage functional that involves a tessellation of the domain and the locations of vehicles within the tesselation. This results in a high-dimensional optimization problem that has to be solved in real time. In our approach we achieve coverage (alternative terminologies are balanced or anti-consensus configurations) through swarming by artificial potentials (see [30, 39] and also, the recent review by [13]). In a related problem, artificial potentials have been used for containment of follower agents within the convex hull of leaders ([38, 6]).

Reachability analysis as a safety verification tool has been studied extensively in the past several decades ([2, 22, 12]). In particular, Hamilton-Jacobi (HJ) reachability ([43, 11]) has seen success in applications such as collision avoidance ([24, 10]), air traffic management ([34, 9]), and emergency landing ([1]). HJ reachability analysis is based on dynamic programming, and involves solving an HJ partial differential equation (PDE) to compute a backward reachable set (BRS) representing the set of states from which danger is inevitable. Safety can therefore be guaranteed, despite the worst-case actions of another agent, by using the derived optimal controller when the system state is on the boundary of the BRS.

Before introducing the specific safe domain coverage problem of interest, we review some of the existing aggregation models, some useful mathematical tools like the LaSalle invariance principle and the concept of signed distance to given domains, and the basic Hamilton-Jacobi reachability theory for addressing pairwise collision avoidance.

1.1 Aggregation models

In this section we introduce some mathematical models for aggregation and collective motion of similar agents; These are also called swarming models. We first describe one model based on self-propelling forces and attraction-repulsion interactions, and then another describing individuals movement alignment. In both cases we comment on the effects of the inclusion of leaders.

1.1.1 Self-propelling, Attraction-Repulsion Model

Consider a group of N agents (e.g. vehicles, particles or biological individuals) with positions $p_1, \cdots, p_N \in \mathbb{R}^n$. With the equation of motion for the i-th individual:

$$\dot{p}_i = v_i, \qquad \dot{v}_i = a_v v_i - \sum_{j \neq i}^{N} \nabla V_I \left(\|p_{ij}\| \right), \tag{1.1}$$

where a_v is a constant, $p_{ij} := p_i - p_j$, is the difference in position between the i-th and j-th individuals, and V_I is an inter-agent potential that models the repulsion and attraction interactions between agents.

The term associated to a_v models either self-propulsion of individuals when a_v is positive or friction when it is negative. Some variants of this model also include extra friction forces following the Rayleigh's law in an effort to compensate the self-propulsion when a_v is positive [19], this balance makes the agents reach asymptotic speeds, without influencing velocity orientation. Although the inter-individual interactions are simple, the emergent formations of these type of models can be complex, showing very inspiring self-organizing patterns like rings, clumps of flocks, single and double mills, as shown in Figure 1.1.

The attractive and repulsive interactions between agents are defined as the gradient of a inter-agent potential $V_I : \mathbb{R}^n \to \mathbb{R}$ that measures the artificial potential energy associated to two vehicles based on their relative distances. Some choices of this are the Morse or generalized Lennard-Jones potentials:

$$V_I^M(x) = \frac{1}{N}\left(-C_A e^{-x/l_A} + C_R e^{-x/l_R}\right); \qquad V_I^{LJ}(x) = \frac{1}{N}\left(-\frac{C_A}{x^\beta} + \frac{C_R}{x^\delta}\right). \tag{1.2}$$

When choosing one of these potentials, the accelerations are defined in terms of the negative of its gradient as in Equation (1.1). This implies that the positive and negative signs in front of each term determine if they are repulsive or attractive interactions respectively. The positive constants C_A and C_R indicate the strength of these attractive and repulsive forces. On the other hand, the l_A and l_R parameters determine the rate of decay of these forces in the case of the Morse potential.

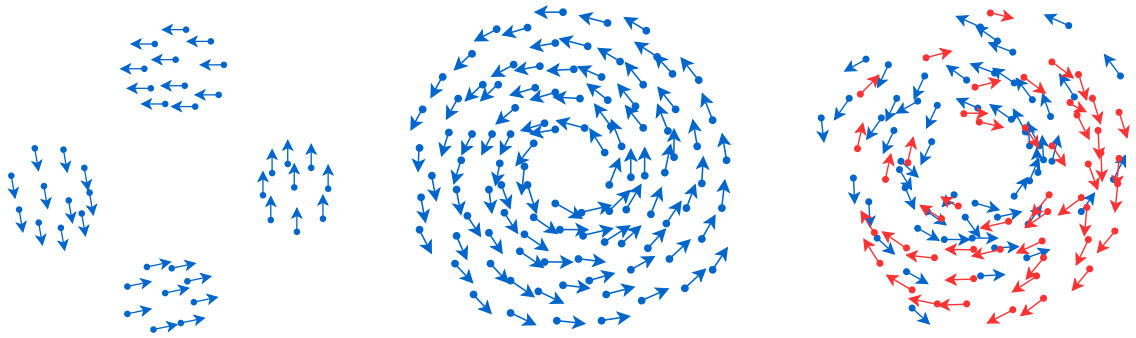

(a) Clumps (b) Mill (c) Double mill

Figure 1.1: Some swarm emergent behaviors of the self-propelling, friction and attraction-repulsion model. The individuals move in: (a) Clumps within which the agents align their velocities forming flocks. (b) Mills, a concentric formation rotating in the same direction. And (c) Double Mills, two mills rotating in opposite directions. Figures (b) and (c) adapted by permission from Springer [7] © (2010). Figure (a) adapted by permission from [19] © (2006).

Inclusion of Leaders

An artificial leader (or just leader) is a virtual point of reference that interacts with other agents and represents group objectives. These interactions based on artificial potentials are used to modify the group formation and direct its motion [30, 36].

An extension of the dynamics for the i-th agent (1.1) in presence of one leader is described by the model

$$\dot{p}_i = v_i, \qquad \dot{v}_i = a_v v_i - \sum_{j \neq i}^{N} \nabla V_I \left(\|p_{ij}\| \right) - \nabla V_h \left(\|h_i\| \right), \tag{1.3}$$

where h_i is the difference in position between the i-th individual and the leader, and V_h is an artificial potential describing the spatial interaction between agents and the leader. Morse or generalized Lennard-Jones potentials (Equation (1.2)) are possible choices for this type of potential.

When a_v is negative, the total energy of system (potential plus kinetic) can be used as Lyapunov function to show that under certain potentials the model (1.3) leads to locally stable dynamics [30].

1.1.2 Cucker-Smale Model

The Cucker-Smale model describes movement alignment between individuals. This model adjusts an agent heading based on the weighted average of the relative velocities respect to the others. The strength of the contribution of a neighbor in the alignment depends on its relative distance, the closer the stronger.

Consider a group of N individuals with positions $p_1, \cdots, p_N$, and velocities $v_1, \cdots, v_N$, the equation of motion for the i-th agent is the following:

$$\dot{p}_i = v_i, \qquad \dot{v}_i = -\sum_{i=1}^{N} f_{al}\left(\|p_{ij}\|\right) v_{ij} \tag{1.4}$$

where $p_{ij} := p_i - p_j$ and $v_{ij} := v_i - v_j$, are the position and velocity differences between the i-th and j-th agents respectively, and $f_{al}(x)$ is a non-negative function called communication rate between agents. Some choices of this function in the literature are the Cucker-Smale and the Vicsek comunication rates [16, 42] respectively:

$$f_{al}^{CS}(x) = \frac{1}{N}\frac{1}{(1+s^2)^{\beta}}, \quad \beta \geq 0; \qquad f_{al}^{V}(x) = \begin{cases} \frac{1}{N}, & \text{if } \|x\| \leq R \\ 0, & \text{if } \|x\| > R. \end{cases} \tag{1.5}$$

In [26], the authors propose the two Lyapunov functions from the kinetic and potential energies given by:

$$\mathcal{E}_{\pm} = \|v\| \pm \int_{\|p_0\|}^{\|p(t)\|} f_{al}(s)\, ds.$$

This is used to show that for initial conditions with small energy the system (1.4) leads to cohesive groups of individuals with same velocity called flocks.

Inclusion of Leaders

The Cucker-Smale model (1.4) can be described from a more general perspective in terms of the set of neighbors affecting the i-th agent, denoted by $\mathcal{N}_i$, as:

$$\dot{p}_i = v_i, \qquad \dot{v}_i = -\sum_{j \in \mathcal{N}_i} f_{al}\left(\|p_{ij}\|\right) v_{ij}. \tag{1.6}$$

The concept of leadership in this model is inspired by the emergent leadership in biological systems, where the leaders guide and promote certain group objectives. The leadership relations between individuals can be hierarchical [40], where the command is shared in different levels, or rooted [25, 31], where the hierarchy is fully dropped and the command is taken only by one individual.

From the perspective of the rooted leadership, the i-th agent, denoted by Q_i, is a leader if $\mathcal{N}_i = \emptyset$ and $Q_i \in \mathcal{N}_j$ for every other j. In other words, if it is not affected by any agent, but affects all of them. Note that as the leader does not experience any interaction, it has not acceleration and therefore its velocity remains constant through time.

The authors in [25] show that for strong enough communication rates between individuals, the agents asymptotically tend to reach a translational motion with constant velocity matching the leader's velocity.

The Cucker-Smale model can be generalized to describe the cone of vision phenomena or partial visual perception [7] in several contexts (e.g. [20, 21]). Some variants of the Cucker-Smale model also include attractive and repulsive forces to guarantee collision avoidance [17, 41, 37] or flocking in the presence of obstacles [36].

1.2 LaSalle Invariance Principle

An useful tool to determine the stability of an autonomous system

$$\dot{x} = X(x), \tag{1.7}$$

satisfying the necessary conditions for existence and uniqueness of their solutions, is the LaSalle invariance principle.

Lemma 1.2.1 (LaSalle Invariance principle [29].)**.** *Let K be a compact set with the property that every solution of* (1.7) *which starts in K remains for all future times in K. Suppose there is a scalar function $\Phi(x)$ which has continuous first partial derivatives in K and is such that $\dot{\Phi}(x) \leq 0$ in K. Let E be the set of all points in K where $\dot{\Phi}(x) = 0$. Let M be the largest invariant set in E. Then every solution starting in K approaches M as $t \to \infty$.*

This widely used principle in the multi-agent literature (see [30, 36, 14]) will be fundamental later in our study to show stability of the resultant collective behaviors.

1.3 Signed Distance

An oriented measure of how far a point x is from a given domain Ω is the signed distance, defined by

$$b(x) = \begin{cases} \min\limits_{x_p \in \partial\Omega} \|x - x_p\|, & \text{if } x \notin \Omega \\ -\min\limits_{x_p \in \partial\Omega} \|x - x_p\|, & \text{if } x \in \Omega. \end{cases}$$

If $\nabla b(x)$ exists, then there exists a unique $P_{\partial\Omega}(x) \in \partial\Omega$, called the projection of x on $\partial\Omega$, such that

$$b(x) = \begin{cases} \|P_{\partial\Omega}(x) - x\|, & \text{if } x \notin \Omega \\ -\|P_{\partial\Omega}(x) - x\|, & \text{if } x \in \Omega \end{cases} \tag{1.8}$$

and

$$\nabla b(x) = \frac{x - P_{\partial\Omega}(x)}{b(x)}. \tag{1.9}$$

Notice that the existence of $\nabla b(x)$ requires the uniqueness of the projection of x on $\partial\Omega$.

1.4 Hamilton-Jacobi Reachability

Consider the two-player differential game described by the joint system

$$\dot{z}(t) = f(z(t), u(t), d(t)) \tag{1.10}$$

$$z(0) = x,$$

where $z \in \mathbb{R}^n$ is the joint state of the players, $u \in \mathcal{U}$ is the control input of Player 1 (hereafter referred to as "control") and $d \in \mathcal{D}$ is the control input of Player 2 (hereafter referred to as "disturbance") .

We assume $f : \mathbb{R}^n \times \mathcal{U} \times \mathcal{D} \to \mathbb{R}^n$ is uniformly continuous, bounded, and Lipschitz continuous in z for fixed u and d, and $u(\cdot) \in \mathcal{U}$, $d(\cdot) \in \mathcal{D}$ are measurable functions. Under these assumptions we can guarantee the dynamical system (1.10) has a unique solution.

In this differential game, the goal of player 2 (the disturbance) is to drive the system into some target set using only non-anticipative strategies [43], while player 1 (the control) aims to drive the system away from it.

We introduce the *time-to-reach* problem as follows.

(Time-to-reach) *Find the time to reach a target set Γ from any initial state x, in a scenario where player 1 maximizes the time, while player 2 minimizes the time. Player 2 is restricted to using non-anticipative strategies, with knowledge of player 1's current and past decisions. Such a time is denoted by $\phi(x)$.*

Following [43], the time to reach a closed target set Γ with compact boundary, given $u(\cdot)$ and $d(\cdot)$ is defined as

$$T_x[u, d] = \min\{t |\ z(t) \in \Gamma\},$$

and the set of non-anticipative strategies as

$$\Theta = \{\theta : \mathcal{U} \to \mathcal{D} |\ u(\tau) = \hat{u}(\tau)\ \forall \tau \le t \Rightarrow$$

$$\theta[u](\tau) = \theta[\hat{u}](\tau)\ \forall \tau \le t\}.$$

Given the above definitions, the *Time-to-reach* problem is equivalent to the differential game problem as follows:

$$\phi(x) = \min_{\theta \in \Theta} \max_{u \in \mathcal{U}} T_x[u, \theta[u]].$$

The collection of all the states that are reachable in a finite time is the capturability set $\mathcal{R}^* = \{x \in \mathbb{R}^n |\ \phi(x) < +\infty\}$.

Applying the dynamic programming principle, as done in [3], we can obtain ϕ as the viscosity solution for the following stationary HJ PDE:

$$\min_{u\in\mathcal{U}} \max_{d\in\mathcal{D}} \{-\nabla\phi(z)\cdot f(z,u,d)-1\}=0, \quad \text{in } \mathcal{R}^*\backslash\Gamma \tag{1.11}$$

$$\phi(z)=0, \quad \text{on } \Gamma.$$

A function is a solution for this HJ PDE in the viscosity sense if it satisfies the following definition.

Definition 1.4.1 (Viscosity solution [4])**.** *A continuous function ϕ is called a viscosity solution of the stationary HJ PDE* (1.11) *if:*

(i) $\phi=0$ *on* Γ*, and*

(ii) for any $v\in C^1(\mathcal{R}^*)$*, if* x *is a local maximum point for* $\phi-v$*, then*

$$\min_{u\in\mathcal{U}} \max_{d\in\mathcal{D}} \{-\nabla v(x)\cdot f(x,u,d)-1\}<0,$$

and

(iii) for any $v\in C^1(\mathcal{R}^*)$*, if* x *is a local minimum point for* $\phi-v$*, then*

$$\min_{u\in\mathcal{U}} \max_{d\in\mathcal{D}} \{-\nabla v(x)\cdot f(x,u,d)-1\}>0.$$

Any ϕ satisfying (ii) is called a viscosity subsolution of (1.11) *whereas, if (iii) holds, it is a viscosity supersolution.*

Previously, this PDE has typically been solved using finite difference methods such as the Lax-Friedrichs method [43].

From the solution $\phi(x)$ we can obtain the control input for optimal avoidance, i.e. the evader's control to maximize the time to collision assuming worst possible disturbance, as

$$u^*(z)=\arg\min_{u\in\mathcal{U}} \max_{d\in\mathcal{D}} \{-\nabla\phi(z)\cdot f(z,u,d)-1\}. \tag{1.12}$$

1.5 Contributions

We develop a new approach to self-collective coordination of autonomous agents/vehicles that aim to reach and cover a moving target domain. We consider two types of vehicle dynamics in the horizontal plane (to be defined formally later) which differ in the nature of the allowed control actions. The first one is the double integrator dynamics, which allows the controller specify the x and y accelerations at any time; among others, it is a simplified model for quadcopter drones. The second type is the planar fixed-wing aircraft dynamics,

for which the control inputs are the vehicle acceleration and its turn rate; those are natural models for cars, bicycles or planes.

The main factors that we consider in our approach are: i) reach and spread over the target domain without having set *a priori* the coverage configuration and the final state of each vehicle, ii) have a distributed control of vehicles, that allows for self-organization and intelligence to emerge at the group level, and (iii) guarantee collision-avoidance throughout the coordination process.

In this aim, we consider a control system that includes both a coverage and a safety controller. The coverage controller is designed to bring the vehicles inside and spread them over the target domain, as well as to align their velocities with those of their neighbors and the moving domain, while the second guarantees collision avoidance of vehicles. In particular, the coverage controller uses two types of artificial potentials and two velocity alignment terms resembling the Cucker-Smale model with single leader. One potential is for inter-individual forces which are designed to achieve a certain desired inter-vehicle spacing as in [30]. Such controller enables emergent self-collective behaviour of the vehicles, similar to the highly coordinated motions observed in biological groups (e.g., flocks of birds, schools of fish); see [5]. The other artificial potential is used for vehicle-target forces by which vehicles reach the target and cover it. The Cucker-Smale terms promote the vehicles to match the velocity of the target domain, which acts as leader.

We emphasize that the coverage controller proposed here (which also includes the approach to the target) is done through agent swarming; there is no leader and no order among the agents. This feature offers robustness to the controller, as it does not have to rely on the well functioning of each individual agent. Self-collective and cooperative behaviour in systems of interacting agents have been of central interest in physics and biology literature (see [42, 15, 19, 16, 21]). A collaborative robot search and target location (without coverage) based on a swarming model was done in [32].

Our vehicle models are second-order, in the sense that agents are implicitly or explicitly controlled through their acceleration; this is to be contrasted with first-order models, where the control inputs are the agents' velocities. We set *a priori* bounds on the control forces, making our controller more realistic than previous approaches, where infinite forces were needed to guarantee collision avoidance ([30, 28]). For an illustration, we show in Figure 1.2 the initial and final states for a simulation using our controller for $N = 10$ vehicles that cover a moving triangular domain.

The safety controller for vehicles with double integrator dynamics is derived from HJ reachability analysis. Unlike the typical approach of numerically solving an associated Hamilton-Jacobi-Isaacs (HJI) PDE, we derive the analytical solution to the PDE to eliminate numerical errors and computation bounds. While multi-vehicle collision avoidance is in general intractable, for vehicles with the double integrator dynamics we observe drastically reduced collision rate by just considering pairwise interactions.

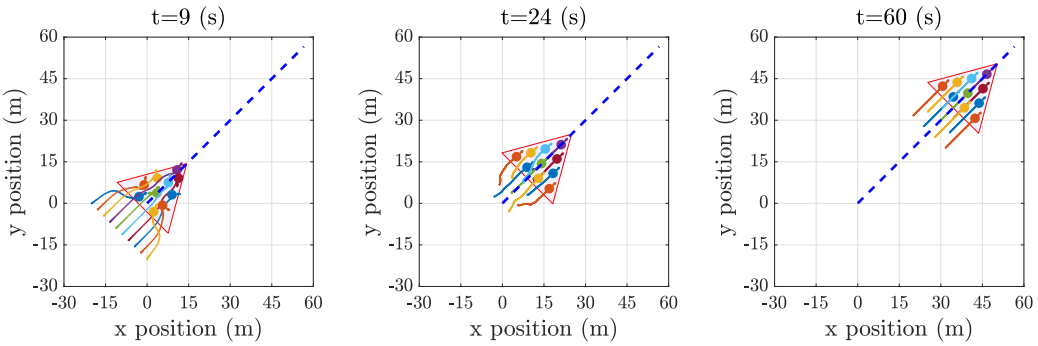

(a) (b) (c)

Figure 1.2: Ten vehicles covering and following a moving triangular domain. Vehicles start in linear formation.

Summarizing, our contributions in this thesis are:

1. We propose a self-collective coordination model for coverage of moving compact domains by vehicles with double integrator dynamics based on existing aggregations models between particles with the novel addition of interaction forces between particles and the target domain, as if the domain were acting as a leader. We validate the results of our approach through numerical simulations.

2. We integrate the HJ reachability analysis in the aggregation model to guarantee pairwise collision avoidance in the case of bounded accelerations for vehicles with double integrator dynamics. We obtain an analytical solution for the resulting PDE, eliminating the numerical errors and computational constraints typical of the numerical solutions.

3. We also propose a methodology for coverage of moving domains by vehicle with planar fixed-wing aircraft dynamics based on an original transformation and tresholding mechanism of our double integrator coverage control policy. We verify that we obtain successful results through numerical simulations.

The work mentioned in contributions 1 and 2 when considering static domains was included in the already accepted conference paper [8], written in collaboration with Professors Razvan Fetecau and Mo Chen. The code implementing all the numerical simulations in this thesis is available at https://github.com/juandados/self-propelling.

The rest of this thesis is organized as follows. In Chapter 2, we present a control algorithm solving the safe coverage problem for static domains in the case of vehicles with double integrator dynamics, as well as theoretical results in stability and collision avoidance verified by numerical simulations. In Chapter 3 we generalize the proposed control policy to one able to deal with moving domains following inertial trajectories. We study its stability and safety properties, while presenting three simulation scenarios illustrating the technique. In

Chapter 4, we formulate a control algorithm for coverage of domains moving along inertial paths for vehicles with fixed-wing aircraft dynamics. We revisit the simulation scenarios in Chapter 3 to illustrate the results. Finally, we make concluding remarks and discussion of the open problems and potential future directions of research.

Chapter 2

Coverage of a static domain

2.1 Problem formulation

We consider a group of N vehicles, each of them denoted as Q_i, $i = 1, \ldots, N$, with the double integrator dynamics described by

$$\dot{p}_i = v_i, \quad \dot{v}_i = u_i; \qquad \|v_i\| \leq v_{max}, \, \|u_i\| \leq u_{max}. \tag{2.1}$$

Here, $p_i = (p_{i,x}, p_{i,y})$ and $v_i = (v_{i,x}, v_{i,y})$ are the position and velocity of Q_i respectively, and $u_i = (u_{i,x}, u_{i,y})$ is the control force applied to this mobile agent.

We consider a vehicle safe if there is no other vehicle closer than a predefined collision radius c_r, in other words, if

$$\|p_i - p_j\| > c_r, \qquad \text{for any } j \neq i. \tag{2.2}$$

In this thesis we are interested in a certain configuration of the group of agents with respect to the domain Ω. Specifically, we adopt the following definitions.

Definition 2.1.1 (r-Subcover)**.** *A group of agents is an* r***-subcover*** *for a compact domain* $\Omega \subseteq \mathbb{R}^2$ *if:*

1. *The distance between any two vehicles is at least* r*.*
2. *The signed distance from any vehicle to* Ω *is less than equal to* $-\frac{r}{2}$*.*

Definition 2.1.2 (r-Cover)**.** *An* r*-subcover for* Ω *is an* r***-cover*** *for* Ω *if its size is maximal (i.e., no larger number of agents can be an* r*-subcover for* Ω*).*

The r-subcover definition is closely related to finding a way to pack circular objects of radius $\frac{r}{2}$ inside of a container with shape Ω. Having an r-cover implies the container is full and there is no room for more of such objects.

The following safe domain coverage problem is of main interest to our work in this chapter.

Safe-domain-coverage by vehicles with double integrator dynamics: *Consider a compact domain Ω in the plane and N vehicles each with dynamics described by* (2.1)*, starting from safe initial conditions. Find the maximal $r > 0$ and a control policy that leads to a stable steady state which is an r-cover for Ω, while satisfying the safety condition* (2.2) *at any time.*

The controller we design and present below has two components. First, each vehicle in the group evolves according to a coverage controller that consists in interaction forces with the rest of the vehicles and with the boundary of the target domain, as well as in braking forces in the current direction of motion. Second, a safety controller, based on Hamilton-Jacobi reachability theory, activates when two vehicles come within an unsafe region with respect to each other. The desired distance r is built into the coverage controller by means of artificial potentials. For certain setups we prove that our proposed coverage control strategy is asymptotically stable, which leads to an r-cover for the domain when this is admissible.

2.2 Coverage controller

Define $p_{ij} := p_i - p_j$, and denote by $P_{\partial\Omega}(p_i)$ the closest point of $\partial\Omega$ to p_i (i.e., the projection of p_i on $\partial\Omega$). Also, define $h_i := p_i - P_{\partial\Omega}(p_i)$, and denote by $[[h_i]]$ the signed distance of p_i from $\partial\Omega$; see Figure 2.1.

The proposed control force is given as

$$u_i = -\sum_{j\neq i}^{N} f_I\left(\|p_{ij}\|\right)\frac{p_{ij}}{\|p_{ij}\|} - f_h\left([[h_i]]\right)\frac{h_i}{[[h_i]]} + f_{v_i}\left(\|v_i\|\right)\frac{v_i}{\|v_i\|}, \tag{2.3}$$

where the three terms in the right-hand-side represent inter-vehicle, vehicle-domain, and braking forces, respectively. We assume each vehicle is able to measure its distance to the target domain, its speed, as well as its position relative to other vehicles. Figure 2.1 illustrates the control forces for two generic vehicles located at p_i and p_j. Shown there are the unit vectors in the directions of the inter-vehicle and vehicle-domain forces (yellow and blue arrows, respectively), along with the resultant that gives the overall control force (red arrows). Note that due to the nonsmoothness of the boundary, different points may have different types of projections: p_i projects on the foot of the perpendicular to $\partial\Omega$, while p_j projects on a corner point of $\partial\Omega$.

We assume the following forms for the functions f_I, f_h and f_{v_i} that appear in the various control forces in Equation (2.3). Figure 2.2 shows the inter-vehicle force f_I and the vehicle-domain force f_h. Note that $f_I(r)$ is negative for $r < r_d$, and zero otherwise. This means that for two vehicles within distance $0 < r < r_d$ from each other, their inter-vehicle interactions are repulsive, while two vehicles at distance larger than r_d apart do not interact at all. The

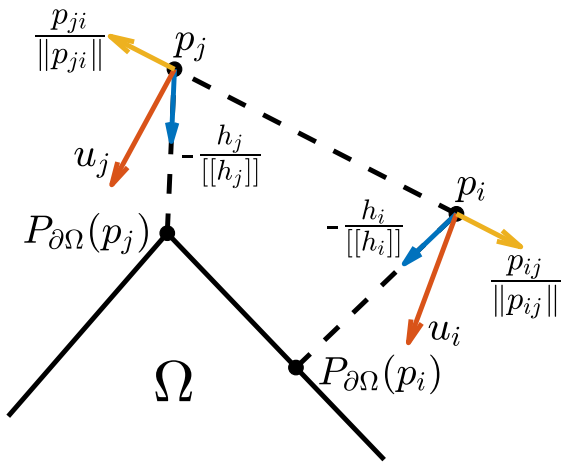

Figure 2.1: Illustration of control forces acting on two vehicles located at p_i and p_j.

vehicle-domain force $f_h(r)$ is zero for $r < -\frac{r_d}{2}$, and positive for $r > -\frac{r_d}{2}$. For a vehicle i outside the target domain, i.e., with $[[h_i]] > 0$, this results in an attractive interaction force toward $\partial\Omega$. On the other hand, for a vehicle inside the domain, where $[[h_i]] < 0$, one distinguishes two cases: i) the vehicle is within distance $\frac{r_d}{2}$ to the boundary, in which case it experiences a repulsive force from it, or ii) the vehicle is more than distance $\frac{r_d}{2}$ from the boundary, in which case it does not interact with the boundary at all. Finally, we take $f_{v_i}(\|v_i\|)$ to be negative to result in a braking force; a specific form of f_{v_i} will be chosen below for analytical considerations (see Equation (2.8)).

An important ingredient of our controller is that one can associate a Lyapunov function to it and hence, investigate analytically the stability of its solutions. We address these considerations now.

Lemma 2.2.1. *The vehicle-domain force* $-f_h([[h_i]])\frac{h_i}{[[h_i]]}$ *and the inter-vehicle force* $-f_I(\|p_{ij}\|)\frac{p_{ij}}{\|p_{ij}\|}$ *are conservative.*

Proof. Let us consider the potential

$$V_h(p_i) = \int_{-\frac{r_d}{2}}^{[[h_i]]} f_h(s)\, ds,$$

which satisfies

$$\nabla_i V_h(p_i) = f_h([[h_i]])\nabla([[h_i]]) = f_h([[h_i]])\frac{h_i}{[[h_i]]}.$$

where we have used the identity $\nabla([[h_i]]) = \frac{h_i}{[[h_i]]}$ (see Theorem 5.1(iii) in [18]).

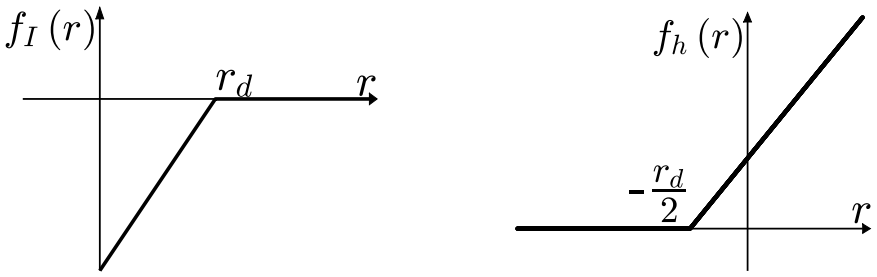

Figure 2.2: Inter-vehicle and vehicle-domain control forces.

Similarly, it can be shown that the inter-vehicle force is the negative gradient of the potential

$$V_I(p_{ij}) = \int_{r_d}^{\|p_{ij}\|} f_I(s)\, ds.$$

□

The potentials corresponding to the interaction forces from Figure 2.2 are shown in Figure 2.3. Their explicit expressions are given by:

$$V_I(x) = \begin{cases} \frac{a_I}{2}(\|x\| - r_d)^2 & \text{for } \|x\| < r_d, \\ 0 & \text{for } \|x\| \geq r_d, \end{cases} \tag{2.4}$$

and

$$V_h(x) = \begin{cases} 0 & \text{for } [[x - P_{\partial\Omega}x]] \leq -\frac{r_d}{2}, \\ \frac{a_h}{2}([[x - P_{\partial\Omega}x]] + \frac{r_d}{2})^2 & \text{for } [[x - P_{\partial\Omega}x]] > -\frac{r_d}{2}, \end{cases} \tag{2.5}$$

where $a_I > 0$ is the slope of the function f_I on $[0, r_d]$ and $a_h > 0$ is the slope of the function f_h on $[-\frac{r_d}{2}, \infty)$. Note that as a_I and a_h are positive, both potentials V_I and V_h are non-negative.

By Lemma 2.2.1, the control given in Equation (2.3) becomes

$$u_i = \sum_{j \neq i}^{N} - \nabla_i V_I(p_{ij}) - \nabla_i V_h(p_i) + f_{v_i}(\|v_i\|) \frac{v_i}{\|v_i\|}. \tag{2.6}$$

Asymptotic behaviour of the controlled system. Consider the following candidate for a Lyapunov function, consisting in kinetic plus (artificial) potential energy:

$$\Phi = \frac{1}{2}\sum_{i=1}^{N}\Big(\dot{p}_i \cdot \dot{p}_i + \sum_{j \neq i}^{N} V_I(p_{ij}) + 2V_h(p_i)\Big). \tag{2.7}$$

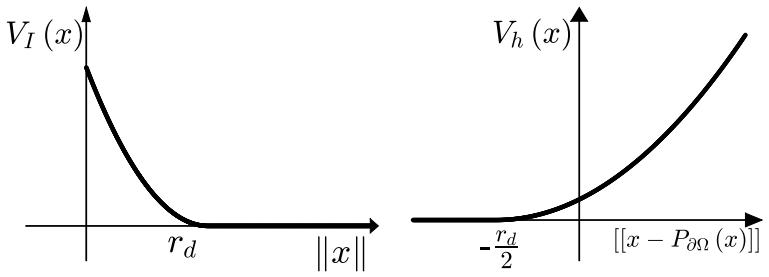

Figure 2.3: Inter-vehicle and vehicle-domain potentials.

Note that each term in Φ is non-negative, and Φ reaches its absolute minimum value when the vehicles are totally stopped. Also, at the global minimum $\Phi = 0$, the equilibrium configuration is an r_d-subcover of Ω; in particular, all vehicles are inside the target domain.

The derivative of Φ with respect to time can be calculated as:

$$\begin{aligned}\dot{\Phi} &= \sum_{i=1}^{N} \dot{p}_i \cdot \left(u_i + \sum_{j \neq i}^{N} \nabla_i V_I\left(p_{ij}\right) + \nabla_i V_h\left(p_i\right) \right) \\ &= \sum_{i=1}^{N} \dot{p}_i \cdot f_{v_i}\left(\|v_i\|\right) \frac{v_i}{\|v_i\|} \\ &= \sum_{i=1}^{N} f_{v_i}\left(\|v_i\|\right) \|v_i\|,\end{aligned}$$

where we used the dynamics (2.1) and equation (2.6). Thus, if we choose

$$f_{v_i}(\|v_i\|) = -a_{v,i} \|v_i\|, \quad \text{with } a_{v,i} > 0, \quad i = 1, \ldots, N, \tag{2.8}$$

then $\dot{\Phi}$ is negative semidefinite and equal to zero if and only if $\dot{p}_i = 0$ for all i (i.e., all vehicles are at equilibrium).

We first use the Lyapunov function to show that the group of vehicles remain within a compact set through time evolution. The key idea is that the vehicle-domain potential V_h is confining the vehicles, and keeps them as a group, as opposed to having them disperse in space [36].

Proposition 2.2.2. *Solutions of* (2.1)*, with control law given by* (2.6) *and* (2.8)*, remain cohesive through time, i.e., there exists an $R > 0$ such that $\|p_i(t)\| \leq R$ for all i and $t \geq 0$.*

Proof. Using that the kinetic energy and the potential V_I are non-negative, and Φ given by (2.7) is non-increasing, we have:

$$\sum_{i=1}^{N} V_h\left(p_i(t)\right) \leq \Phi(t) \leq \Phi(0).$$

To show boundedness of p_i we only need to consider the case $p_i \notin \Omega$, as otherwise the vehicles are inside the compact set Ω. Using the expression (2.5) for V_h, we then find:

$$\frac{a_h}{2}\sum_{i=1}^{N}\left(\|p_i(t) - P_{\partial\Omega}p_i(t)\| + \frac{r_d}{2}\right)^2 \leq \Phi(0).$$

This shows that the distances from $p_i(t)$ to the domain Ω remain bounded by $\sqrt{\frac{2\Phi(0)}{a_h}}$ when $p_i \notin \Omega$, therefore, there exists $R > 0$ such that $\|p_i(t)\| \leq R$, for all i and $t \geq 0$. □

Remark 2.2.3. *From LaSalle Invariance Principle we can conclude that the controlled system approaches asymptotically an equilibrium configuration. By the expressions* (2.6) *of the control force and* (2.7) *of the Lyapunov function, these are equilibria that are critical points of the artificial potential energy* $\frac{1}{2}\sum_{i=1}^{N}\left(\sum_{j\neq i}^{N} V_I\left(p_{ij}\right) + 2V_h\left(p_i\right)\right)$*. We expect that any critical point other than the local minima (e.g., saddles or local maxima) are unstable [36], and hence, almost every solution of the system will approach asymptotically a local minimum of the potential energy.*

For certain simple setups (e.g., a square number of vehicles in a square domain – see Figure 2.5b, or a triangular number of vehicles in a triangular domain), the r_d-covers are isolated equilibria. Hence, together with the fact that such equilibria are global minimizers for Φ, their local asymptotic stability can be inferred. The formal result is given by the following proposition.

Proposition 2.2.4. *Consider a group of N vehicles with dynamics defined by* (2.1)*, and the control law given by* (2.6) *and* (2.8)*. Let the equilibrium of interest be of the form $\dot{p}_i = 0$, $\|p_{ij}\| \geq r_d$ and $[[h_i]] \leq -\frac{r_d}{2}$ for $i, j = 1, \cdots, N$ (see Definitions 2.1.1 and 2.1.2), and assume that this equilibrium configuration is isolated. Also assume that there is a neighborhood about the equilibrium in which the control law remains smooth. Then, the equilibrium is a global minimum of the sum of all the artificial potentials and is locally asymptotically stable.*

Proof. This follows from the LaSalle invariance principle and the arguments made above. □

Choosing an adequate r_d when solving the *safe-domain-coverage* problem leads us to a nonlinear optimization problem (see [33]) which can be difficult in itself. Our heuristic approach for picking this parameter relies on the premise that any vehicle is covering roughly the same square area, i.e.,

$$r_d = \sqrt{\frac{Area\left(\Omega\right)}{N}}. \tag{2.9}$$

Note that (2.9) gives the exact formula for the maximal radius when both the number of vehicles and the domain are square, making the r_d-covers isolated equilibria, a key assump-

tion in Proposition 2.2.4. Also, this particular choice for r_d leads to the desired cover for several domains with regular geometries (see Section 2.5).

2.3 Collision avoidance

An important component of our study is the guarantee that vehicles do not collide through the time evolution. In our context this means that vehicles do not come closer than the collision radius c_r (see condition (2.2)). For small initial energies, collision avoidance can be shown directly, using the decay of the Lyapunov function (2.7). For general cases, we introduce a safety controller based on HJ reachability analysis.

Small initial energy. For initial data with small energy Φ we can show that no vehicle collisions can occur. Specifically, the following result hold.

Proposition 2.3.1. *Consider a target domain Ω and a group of N vehicles with dynamics defined by* (2.1) *and* (2.6) *(see also* (2.8)*). Assume the energy $\Phi(0)$ of the initial configuration satisfies*

$$\Phi(0) < \int_{r_d}^{c_r} f_I(s)\, ds = \frac{a_I}{2}(c_r - r_d)^2.$$

Then, no vehicle collision can occur for all $t \geq 0$.

Proof. Suppose by contradiction that there is a time t_* at which vehicles k and l are at collision radius from each other, that is, $\|p_k(t_*) - p_l(t_*)\| = c_r$. Given that V_I is non-negative, the inter-vehicle potential energy at the collision time can be bounded below as:

$$\frac{1}{2}\sum_{i=1}^{N}\sum_{j\neq i}^{N} V_I\left(p_{ij}(t_*)\right) \geq V_I(p_k(t_*) - p_l(t_*)) = \int_{r_d}^{c_r} f_I(s)\, ds.$$

On the other hand, using that the kinetic energy and the potential V_h are non-negative, we have:

$$\frac{1}{2}\sum_{i=1}^{N}\sum_{j\neq i}^{N} V_I\left(p_{ij}(t_*)\right) \leq \Phi(t_*) \leq \Phi(0).$$

By combining the two sets of inequalities above one finds $\Phi(0) \geq \int_{r_d}^{c_r} f_I(s)\, ds$, which contradicts the assumption on the initial energy $\Phi(0)$. □

The result above can be generalized as follows.

Proposition 2.3.2. *Consider a target domain Ω and a group of N vehicles with dynamics defined by* (2.1)*,* (2.6) *and* (2.8)*. Assume the energy $\Phi(0)$ of the initial configuration satisfies*

$$\Phi(0) < (k+1)\int_{r_d}^{c_r} f_I(s)\, ds,$$

for some $k \in \mathbb{Z}_+$. Then, at most k distinct pairs of vehicles could be possibly unsafe ($k = 0$ guarantees a safe motion) for all $t \geq 0$.

Proof. The proof follows closely the proof of Proposition 2.3.1. Assume by contradiction that $k+1$ pairs of vehicles collide at time t_*, it means their relative distances are less than c_r. Then, on one hand, following the argument in Proposition 2.3.1, we have:

$$\frac{1}{2}\sum_{i=1}^{N}\sum_{j\neq i}^{N} V_I\left(p_{ij}(t_*)\right) \geq (k+1)\int_{r_d}^{c_r} f_I(s)\,ds,$$

where we use the fact that $V_I(p_{ij})$ is a non-increasing radial function.

On the other hand,

$$\frac{1}{2}\sum_{i=1}^{N}\sum_{j\neq i}^{N} V_I\left(p_{ij}(t_*)\right) \leq \Phi(t_*) \leq \Phi(0),$$

leading to a contradiction. □

Note that the two last results assume that the control law (2.6) is applied as it is, it does not take into account the input force constrains in (2.1). The following HJ reachability analysis deals with the input force bounds to guarantee pairwise safety.

Collision avoidance via Hamilton-Jacobi theory. To guarantee pairwise collision avoidance for general configurations (when Proposition 2.3.2 does not apply), we design a safety controller based on HJ reachability analysis.

Consider the dynamics between two vehicles Q_i, Q_j defined in terms of their relative states

$$p_{r,x} = p_{i,x} - p_{j,x}, \qquad v_{r,x} = v_{i,x} - v_{j,x},$$

$$p_{r,y} = p_{i,y} - p_{j,y}, \qquad v_{r,x} = v_{i,x} - v_{j,x},$$

where the vehicle Q_i is the evader, located at the origin, and Q_j is the pursuer, the latter being considered as the model disturbance. In this case the relative dynamical system is given by

$$\begin{aligned} \dot{p}_{r,x} &= v_{r,x} \qquad & \dot{v}_{r,x} &= u_{i,x} - u_{j,x}, \\ \dot{p}_{r,y} &= v_{r,y} \qquad & \dot{v}_{r,y} &= u_{i,y} - u_{j,y}, \end{aligned} \tag{2.10}$$

with $\|u_i\|$,$\|u_j\| \leq u_{max}$, where $u_i = (u_{i,x}, u_{i,y})$ and $u_j = (u_{j,x}, u_{j,y})$ are the control inputs of the agents Q_i and Q_j, respectively. From the perspective of agent Q_i, the control inputs of Q_j, $u_j = (u_{j,x}, u_{j,y})$, are treated as worst-case disturbance.

According to (2.2), the unsafe states are described by the target set $\Gamma = \left\{z : p_{r,x}^2 + p_{r,y}^2 \leq c_r^2\right\}$.

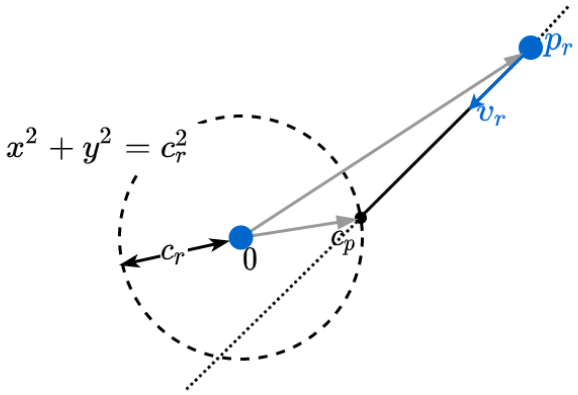

Figure 2.4: Geometric illustration for solving HJI PDE (1.11). Here c_p represents the collision point.

Consider $\psi(z)$ as the time it takes for the solution of the dynamical system (2.10), with starting point $z = (p_{r,x}, v_{r,x}, p_{r,y}, v_{r,y})$ in $\mathcal{R}^* \setminus \Gamma$, to reach Γ when the disturbance and control inputs are optimal. As the two vehicles have the same capabilities we make the educated guess that the optimal non-anticipative strategy for the pursuer is copying the evader accelerations, having so a zero relative acceleration. This implies that the relative velocity will remain constant v_r through time.

If p_r and v_r are such that a collision can occur, there exist a collision point c_p, see Figure 2.4. This will be one of the intersection points of the line crossing through p_r with direction parallel to v_r and the circle of radius c_r centered at the origin. To get the collision time we replace the coordinates of c_p from the perspective of the line, namely $c_p = (p_{r,x} + \psi(z)\, v_{r,x},\, p_{r,y} + \psi(z)\, v_{r,y})$, into the canonical equation of the circle.

Using the above geometric argument one can show that this time is the minimum of the two solutions of the following quadratic equation:

$$\left(v_{r,x}^2 + v_{r,y}^2\right)\psi^2(z) + 2\left(p_{r,x}v_{r,x} + p_{r,y}v_{r,y}\right)\psi(z) + \left(p_{r,x}^2 + p_{r,y}^2 - c_r^2\right) = 0. \tag{2.11}$$

Let us verify first that the minimum of the two solutions satisfies indeed the HJI PDE (1.11).

Proposition 2.3.3. *Consider the function $\psi(z)$ defined as*

$$\psi(z) := \frac{-\left(p_{r,x}v_{r,x} + p_{r,y}v_{r,y}\right) - \sqrt{\Delta}}{v_{r,x}^2 + v_{r,y}^2} \qquad \text{in } \mathcal{R}^* \setminus \Gamma,$$

where

$$\Delta = \left(p_{r,x}v_{r,x} + p_{r,y}v_{r,y}\right)^2 - \left(v_{r,x}^2 + v_{r,y}^2\right)\left(p_{r,x}^2 + p_{r,y}^2 - c_r^2\right).$$

Also define $\psi(z)$ *to be* 0 *on* Γ. *Then* $\psi(z)$ *satisfies equation* (1.11).

Proof. For $z \in \mathcal{R}^* \setminus \Gamma$, $\psi(z)$ is the minimum solution of the quadratic equation (2.11). By using implicit differentiation on (2.11) one can show

$$\frac{\partial \psi}{\partial p_{r,x}} = -\frac{v_{r,x}\psi(z) + p_{r,x}}{\left(v_{r,x}^2 + v_{r,y}^2\right)\psi(z) + (p_{r,x}v_{r,x} + p_{r,y}v_{r,y})}$$

$$\frac{\partial \psi}{\partial p_{r,y}} = -\frac{v_{r,y}\psi(z) + p_{r,y}}{\left(v_{r,x}^2 + v_{r,y}^2\right)\psi(z) + (p_{r,x}v_{r,x} + p_{r,y}v_{r,y})}.$$

To put system (2.10) in the general form (1.10) from Section 1.4, let $z = (p_{r,x}, p_{r,y}, v_{r,x}, v_{r,y})$, $u = (u_x, u_y) := (u_{i,x}, u_{i,y})$, $d = (d_x, d_y) := (u_{j,x}, u_{j,y})$, and let $f(z, u, d)$ represent the right-hand-side of (2.10). Then,

$$\begin{aligned}
&\min_{u\in\mathcal{U}} \max_{d\in\mathcal{D}} \{-\nabla\psi(z) \cdot f(z,u,d) - 1\} \\
&= \min_{u\in\mathcal{U}} \max_{d\in\mathcal{D}} \left\{ -\frac{\partial\psi(z)}{\partial p_{r,x}} v_{r,x} - \frac{\partial\psi(z)}{\partial v_{r,x}}(u_x - d_x) \right. \\
&\qquad\qquad \left. -\frac{\partial\psi(z)}{\partial p_{r,y}} v_{r,y} - \frac{\partial\psi(z)}{\partial v_{r,y}}(u_y - d_y) - 1 \right\} \\
&= -\left(\frac{\partial\psi(z)}{\partial p_{r,x}} v_{r,x} + \frac{\partial\psi(z)}{\partial p_{r,y}} v_{r,y} \right) - 1 \\
&= \frac{(v_{r,x}\psi(z) + p_{r,x})\, v_{r,x} + (v_{r,y}\psi(z) + p_{r,y})\, v_{r,y}}{\left(v_{r,x}^2 + v_{r,y}^2\right)\psi(z) + (p_{r,x}v_{r,x} + p_{r,y}v_{r,y})} - 1 = 0,
\end{aligned}$$

where we have used the fact that $\psi(z)$ is differentiable in $\mathcal{R}^* \setminus \Gamma$ and that the minimum and maximum in the second equal sign are attained at

$$u^* = d^* = u_{max} \frac{\left(\frac{\partial\psi(z)}{\partial v_{r,x}}, \frac{\partial\psi(z)}{\partial v_{r,y}}\right)}{\left\| \frac{\partial\psi(z)}{\partial v_{r,x}}, \frac{\partial\psi(z)}{\partial v_{r,y}} \right\|}, \tag{2.12}$$

and therefore cancel out.

For $z \in \Gamma$ the equation (1.11) is satisfied by the definition of ψ.

□

Note that we have found a differentiable function satisfying the HJI PDE (2.11) in $\mathcal{R}^* \setminus \Gamma$. It can be shown that under these conditions this is a solution in the viscosity sense (see [4] Prop 1.3.).

Similarly as before, by implicit differentiation of (2.11) one can also show

$$\frac{\partial \psi}{\partial v_{r,x}} = \frac{-v_{r,x}\psi^2(z) - p_{r,x}\psi(z)}{\left(v_{r,x}^2 + v_{r,y}^2\right)\psi(z) + (p_{r,x}v_{r,x} + p_{r,y}v_{r,y})} \tag{2.13a}$$

$$\frac{\partial \psi}{\partial v_{r,y}} = \frac{-v_{r,y}\psi^2(z) - p_{r,y}\psi(z)}{\left(v_{r,x}^2 + v_{r,y}^2\right)\psi(z) + (p_{r,x}v_{r,x} + p_{r,y}v_{r,y})}. \tag{2.13b}$$

Now, by using (2.12) we can derive a closed expression for the optimal avoidance controller. Note that to use this pairwise avoidance strategy we require each vehicle to know its speed and position relative to the other vehicles.

For applications using the static HJI PDE (1.11) or similar equations, the solution is commonly approximated via finite difference methods such as the one presented in [43]; however, using an analytic solution leads to two main advantages. First, refinements in the resolution when using uniform grid point spacing may require a large amount of memory and long computational times that scale very poorly. Second, these methods are only able to compute the solution in a bounded domain. Having an analytical solution allows us to have the best possible resolution in an unbounded domain. Practically, this allows us to predict and react to possible collisions arbitrarily far into the future.

2.4 Overall control logic

We have presented two controllers. First, a controller based on virtual potentials which leads to coverage, but without taking into consideration safety; and second, a safety controller that guarantees pairwise collision avoidance. The main objective of this section is to describe how to switch between these two controllers.

We will consider that vehicle Q_i is in potential conflict with vehicle Q_j if the time to collision $\psi(z_i)$ (time to reach Γ), given the relative current state z_i, is less than or equal to a specified time horizon t_{safety}. In other words, a danger is defined when a vehicle is susceptible to collision in the next t_{safety} seconds. In such a case Q_i must use the safety controller, otherwise, the coverage controller is used.

In the case that a vehicle detects more than one conflict, it will apply the control policy of the first conflict detected at that particular time. Algorithm 1 describes the overall control logic for every vehicle Q_i.

In Algorithm 1, lines 6 and 7 can be obtained from equations (2.13a), (2.13b) and (2.12) (also note the normalization step in line 14), while line 12 comes from the explicit coverage control (2.3).

Remark 2.4.1. *It is clear that thresholding the force (Algorithm 1 line 14) the theoretical guarantees may not necessary hold anymore. However, when close to the desired operation*

Input: State x_i of a vehicle Q_i; states $\{x_j\}_{j\neq i}$ of other vehicles $\{Q_j\}_{j\neq i}$; a domain Ω to cover.
Parameter: A time horizon for safety check t_{safety};
Output: A control u_i for Q_i.

$safe \leftarrow$ True;
for $j \neq i$ **do**
  $z \leftarrow x_i - x_j$;
  if $\psi(z) \leq t_{safety}$ **then**
    $safe \leftarrow$ False;
    $U_{ix} = -\frac{v_{r,x}\psi^2(z)+p_{r,x}\psi(z)}{\left(v_{r,x}^2+v_{r,y}^2\right)\psi(z)+(p_{r,x}v_{r,x}+p_{r,y}v_{r,y})}$;
    $U_{iy} = -\frac{v_{r,y}\psi^2(z)+p_{r,y}\psi(z)}{\left(v_{r,x}^2+v_{r,y}^2\right)\psi(z)+(p_{r,x}v_{r,x}+p_{r,y}v_{r,y})}$;
    break for
  end
end
if *safe* **then**
  $(U_{ix}, U_{iy}) = -\sum_{j\neq i}^{N} f_I(\|p_{ij}\|)\frac{p_{ij}}{\|p_{ij}\|} - f_h([[h_i]])\frac{h_i}{[[h_i]]} + f_{v_i}(\|v_i\|)\frac{v_i}{\|v_i\|}$;
end
$u_i = u_{max}\frac{(U_{ix},U_{iy})}{\|(U_{ix},U_{iy})\|}$;
return u_i;

Algorithm 1: Overall control logic for a generic vehicle Q_i.

point the coverage forces are small enough to not be thresholded and it is feasible to apply the required control force, implying the theoretical results are locally valid.

2.5 Numerical simulations

In this section, we show numerical simulations with various domains using the coverage and safety controllers discussed above.

Square domain. We first consider the problem in which several vehicles cover a square domain. Here we present two strategies: while both of them use the coverage controller described in Section 2.2, only the second strategy switches to the safety controller when necessary, according to Section 2.4. In both cases 16 vehicles start from a horizontal line setup outside of the target square domain, as shown in Figure 2.5a.

The left column of Figure 2.6 illustrates different time steps for the scenario when the safety controller is not used, while the right column shows results in the presence of the safety controller. The large coloured dots represent the position of the vehicles, the dashed tails are past trajectories (shown for the previous 5 seconds), and the arrows indicate the movement direction. Note however that we have not shown the arrows when the velocities are very small, as the tails are more meaningful in this case.

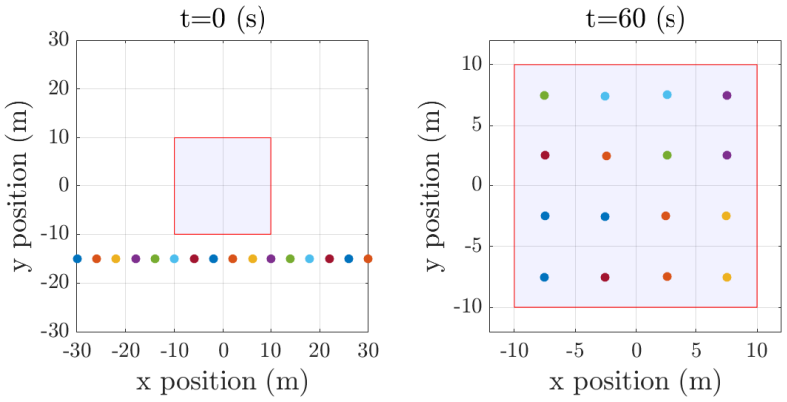

Figure 2.5: Initial (a) and steady (b) states for covering a square domain, with a square number of vehicles ($N = 16$).

At $t = 0$ (s) there are no contributions from the inter-vehicle forces or from the safety controller as the vehicles are far from each other and the initial speed is zero. The only contribution comes from the vehicle-domain forces, which pull the mobile agents toward the interior of the square; see initial trajectory tails in Figures 2.6a and 2.6b. At $t = 5$ (s) the vehicles without safety controller are more prone to collisions due to the symmetry of the initial condition. The safety controller slows down some vehicles hence breaking this symmetry, and allowing them to enter in the crowded area without collisions.

As the forces between vehicles and domain are piece-wise linear with respect to the distance, they can be thought of as spring-like forces; in that respect, the presence of overshoots is expected, as shown in Figure 2.6c. However, Figure 2.6d indicates that in addition to preventing collisions, the use of the safety controller reduces the overshoot considerably.

After $t = 50$ (s) both control strategies reach the steady state shown in Figure 2.5b. We note however that the system with collision avoidance reaches the equilibrium faster, as shown by Figures 2.6e and 2.6f.

A *collision event* starts when the distance between two vehicles is less than or equal to the collision radius c_r, and ends when the distance becomes greater than c_r. The collision event count for the square domain coverage with and without the safety controller, for various number of vehicles, is shown in Table 2.1. It is noteworthy that in the absence of the safety controller the collision count increases significantly with the number of vehicles, while it remains zero or very low when the safety controller is used.

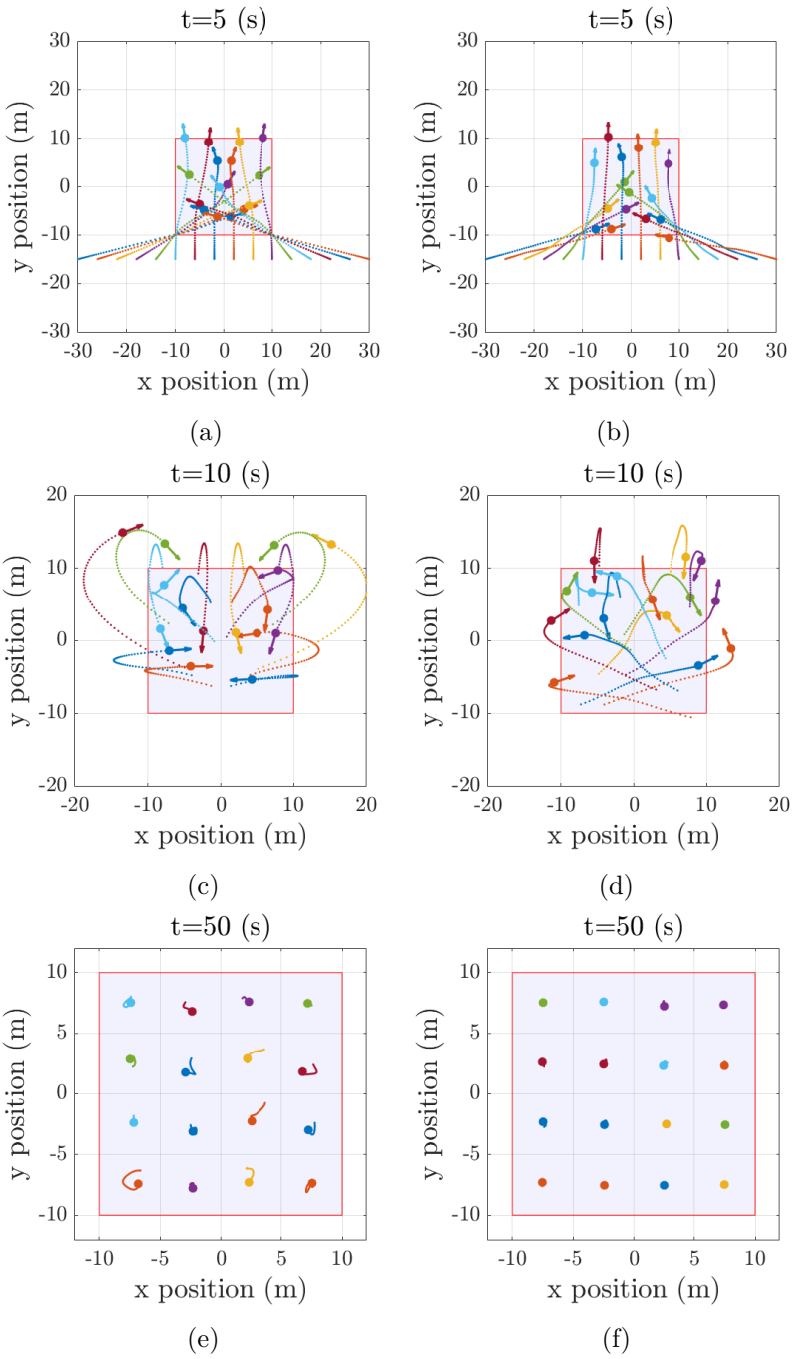

Figure 2.6: Square domain coverage at different time instants, without (left) and with (right) safety controller, when $N = 16$, $c_r = 2\,(\mathrm{m})$, $v_{max} = 10\,(\mathrm{m/s})$, $u_{max} = 3\,(\mathrm{m/s^2})$, $t_{safety} = 5\,(\mathrm{s})$, side length $l = 20\,(\mathrm{m})$, domain area $A = l^2 = 400\,(\mathrm{m^2})$ and $r_d = \sqrt{\frac{A}{N}} = 5\,(\mathrm{m})$. Vehicles start in a horizontal line configuration and reach a square grid steady state which is an r_d-cover of the domain (see Definition 2.1.2). The use of the safety controller reduces both the collision count and the overshoot, and helps reach the steady state faster.

Table 2.1: Square coverage collision count.

number of vehicles	without avoidance	with avoidance
9	8	0
16	51	0
25	146	2

Note that safety issues may arise when a vehicle needs to avoid two or more vehicles at the same time. In this case the pairwise safety approach used in this thesis does not guarantee collision avoidance. Guaranteed collision avoidance for more than two vehicles is an unsolved problem, as explored for example in [10].

Chapter 3

Coverage of a moving domain

3.1 Problem formulation

We consider in this section the coverage problem when the target domain moves with prescribed constant velocity v_d. Specifically, let $\Omega \subseteq \mathbb{R}^2$ be a compact domain and define $\Omega_t = \Omega + tv_d$, representing the moving domain at time t. Alternatively, if one sets an arbitrary marker point p_d (e.g., the centre of mass) in Ω, its motion is given by $p_d(t) = p_d + tv_d$.

We are interested in covering the domain Ω_t (see Definitions 2.1.1 and 2.1.2), which changes through time. For this reason we want the vehicles to reach asymptotically, as $t \to \infty$, the velocity of the target domain, while maintaining a cohesive group through dynamics. This is expressed by the concept of flocking [36, 16, 27].

Consider a group of N vehicles, each of them governed by the double integrator dynamics, i.e.,

$$\dot{p_i} = v_i, \quad \dot{v_i} = u_i, \qquad i = 1, \ldots, N, \tag{3.1}$$

with control u_i to be specified later. We adapt below the definition of flocking from [26] to the problem of moving target.

Definition 3.1.1 (Flocking with a moving target)**.** *A group of vehicles has a time-asymptotic flocking with a target domain moving with constant velocity v_d if its positions and velocities $\{p_i, v_i\}$, $i = 1, \cdots, N$ satisfy the following two conditions:*

1. *The relative positions with respect to the marker point in the domain are uniformly bounded in time (forming a group):*

$$\sup_{0 \le t < \infty} \sum_{i=1}^{N} \|p_i(t) - p_d(t)\|^2 < \infty.$$

2. *The relative velocities with respect to the moving domain go to zero asymptotically in time (velocity alignment):*

$$\lim_{t\to+\infty}\sum_{i=1}^{N}\left\|v_i\left(t\right)-v_d\right\|^2=0,$$

In this case, our safe domain coverage problem of interest is the following:

Safe-domain-coverage by vehicles with double integrator dynamics for moving domains: *Consider a compact domain Ω_t that moves with constant velocity v_d in the plane, and N vehicles with dynamics described by* (3.1)*, starting from safe initial conditions. Find the maximal $r>0$ and a control policy that leads to an r-cover for Ω_t that flocks with the moving target, while satisfying the safety condition* (2.2) *at any time.*

3.2 Coverage controller with alignment

At first glance, one might think that the current coverage policy (2.3) can work well while solving our latest problem of interest since the moving domain will always attract the vehicles to its interior. However, as this approach encourages vehicles to be static, they tend to lag behind the domain, reacting only when they are out of it. This suggests that the vehicles require a mechanism to align their velocities with those of their neighbors and the target domain.

Inspired by the Cucker-Smale model with rooted leadership (see 1.1.2), we propose the control force with inclusion of inter-vehicle and vehicle-domain alignment forces given by:

$$u_i=-\sum_{j\neq i}^{N}f_I\left(\left\|p_{ij}\right\|\right)\frac{p_{ij}}{\left\|p_{ij}\right\|}-f_h\left(\left[\left[h_i\right]\right]\right)\frac{h_i}{\left[\left[h_i\right]\right]}-\underbrace{\sum_{j\neq i}^{N}f_{al}\left(\left\|p_{ij}\right\|\right)v_{ij}}_{\text{inter-vehicle}}-\underbrace{a_v\left(v_i-v_d\right)}_{\text{vehicle-domain}}, \tag{3.2}$$

Where we kept the notations from Chapter 2. i.e., set $p_{ij}:=p_i-p_j$, $v_{ij}:=v_i-v_j$, and denote by $P_{\partial\Omega_t}\left(p_i\right)$ the projection of p_i on $\partial\Omega_t$. Also, $h_i:=p_i-P_{\partial\Omega_t}\left(p_i\right)$, and $\left[\left[h_i\right]\right]$ denotes the signed distance of p_i from $\partial\Omega_t$. In addition, f_{al} is a non-negative communication function and a_v is a positive constant.

The inter-vehicle alignment force controls the alignment of vehicle i's velocity with the velocities of the rest of the vehicles, and the extent to which such alignment occurs depends on the relative distance $\left\|p_{ij}\right\|$ between the interacting vehicles. For a communication function f_{al} that is non-increasing (this is a typical assumption in the literature [27, 26]), vehicles align stronger with their neighbours, and less with vehicles that are further apart. The results presented in this thesis correspond to a communication function in the form:

$$f_{al}\left(\left\|p_{ij}\right\|\right)=C_{al}e^{-\frac{\left\|p_{ij}\right\|}{l_{al}}},$$

where C_{al} and l_{al} are constants associated to the alignment strength and alignment range, respectively. This function was considered in [21] in the context of honeybee swarms.

The vehicle-domain alignment force drives the velocity of the vehicles to the domain's velocity v_d. In this regard, the braking force in the static domain model (see (2.3) and (2.8)) can also be interpreted as an alignment force that brings the vehicles to a stop. Also, while for simplicity we have taken a common constant a_v for all vehicles, the considerations that follow apply to the more general alignment forces $a_{v,i}(v_i - v_d)$, with $a_{v,i} > 0$.

By changing to relative coordinates with respect to the frame of the moving domain, one can recover the case of a stationary domain ($v_d = 0$). Indeed, change variables to:

$$\begin{cases} \tilde{p}_i & := p_i - tv_d, \\ \tilde{v}_i & := v_i - v_d, \end{cases} \tag{3.3}$$

and note that the inter-vehicle positions and velocities are invariant to this change of coordinates, that is,

$$\tilde{p}_{ij} := \tilde{p}_i - \tilde{p}_j = p_{ij},$$

$$\tilde{v}_{ij} := \tilde{v}_i - \tilde{v}_j = v_{ij}.$$

Also, by translation, the distance to the target domain satisfies

$$h_i = p_i - P_{\partial\Omega_t}(p_i) = (p_i - tv_d) - P_{\partial\Omega_t - tv_d}(p_i - tv_d) = \tilde{p}_i - P_{\partial\Omega}(\tilde{p}_i).$$

Hence, in the new variables, the signed distances $[[\tilde{h}_i]]$, where

$$\tilde{h}_i := \tilde{p}_i - P_{\partial\Omega}(\tilde{p}_i), \tag{3.4}$$

are with respect to the initial (fixed) domain Ω.

The observations above allow us to rewrite the control (3.2) in the new variables. We find that in the moving coordinate frame the dynamics of the N vehicles is given by:

$$\dot{\tilde{p}}_i = \tilde{v}_i, \quad \dot{\tilde{v}}_i = \tilde{u}_i, \qquad i = 1, \dots, N,$$

where

$$\tilde{u}_i = -\sum_{j \neq i}^{N} f_I(\|\tilde{p}_{ij}\|) \frac{\tilde{p}_{ij}}{\|\tilde{p}_{ij}\|} - \sum_{j \neq i}^{N} f_{al}(\|\tilde{p}_{ij}\|) \tilde{v}_{ij} - f_h([[\tilde{h}_i]]) \frac{\tilde{h}_i}{[[\tilde{h}_i]]} - a_v \tilde{v}_i.$$

Note that this corresponds to the dynamics in the original variables for a stationary domain.

3.3 Asymptotic behaviour

We first investigate the dynamics with control (3.2) for a stationary target ($v_d = 0$). Using the potentials introduced in (2.4) and (2.5), we write the control as:

$$u_i = -\sum_{j\neq i}^{N} \nabla_i V_I\left(p_{ij}\right) - \nabla_i V_h\left(p_i\right) - \sum_{j\neq i}^{N} f_{al}(\|p_{ij}\|)(v_i - v_j) - a_v v_i. \tag{3.5}$$

Consider the same candidate for a Lyapunov function, consisting in kinetic plus (artificial) potential energy:

$$\Phi = \frac{1}{2}\sum_{i=1}^{N}\Big(\dot{p}_i \cdot \dot{p}_i + \sum_{j\neq i}^{N} V_I\left(p_{ij}\right) + 2V_h\left(p_i\right)\Big).$$

Note that each term in Φ is non-negative, and Φ reaches its absolute minimum value when the vehicles are totally stopped.

The derivative of Φ with respect to time can be calculated as:

$$\begin{aligned}\dot{\Phi} &= \sum_{i=1}^{N} \dot{p}_i \cdot \Big(u_i + \sum_{j\neq i}^{N} \nabla_i V_I\left(p_{ij}\right) + \nabla_i V_h\left(p_i\right)\Big) \\ &= \sum_{i=1}^{N} v_i \cdot \Big(-\sum_{j\neq i}^{N} f_{al}(\|p_{ij}\|)(v_i - v_j) - a_v v_i\Big).\end{aligned} \tag{3.6}$$

For the inter-vehicle alignment term, write

$$\sum_{i=1}^{N} v_i \cdot \sum_{j\neq i}^{N} f_{al}(\|p_{ij}\|)(v_i - v_j) = \frac{1}{2}\sum_{i=1}^{N} v_i \cdot \sum_{j\neq i}^{N} f_{al}(\|p_{ij}\|)(v_i - v_j) + \frac{1}{2}\sum_{j=1}^{N} v_j \cdot \sum_{i\neq j}^{N} f_{al}(\|p_{ji}\|)(v_j - v_i),$$

where in the second term in the right-hand-side we simply renamed $i \leftrightarrow j$ as indices of summation. From there, use that $\|p_{ij}\| = \|p_{ji}\|$ to get:

$$\sum_{i=1}^{N} v_i \cdot \sum_{j\neq i}^{N} f_{al}(\|p_{ij}\|)(v_i - v_j) = \frac{1}{2}\sum_{i=1}^{N}\sum_{j\neq i}^{N} f_{al}(\|p_{ij}\|)\|v_i - v_j\|^2.$$

Hence, from (3.6), we find:

$$\dot{\Phi} = -\frac{1}{2}\sum_{i=1}^{N}\sum_{j\neq i}^{N} f_{al}(\|p_{ij}\|)\|v_i - v_j\|^2 - a_v \sum_{i=1}^{N} \|v_i\|^2.$$

In the case of a target domain moving with velocity v_d, one can change to relative coordinates (3.3) as explained in Section 3.2, and set:

$$\Phi = \frac{1}{2}\sum_{i=1}^{N}\Big(\dot{\tilde{p}}_i \cdot \dot{\tilde{p}}_i + \sum_{j\neq i}^{N} V_I\left(\tilde{p}_{ij}\right) + 2V_h\left(\tilde{p}_i\right)\Big). \tag{3.7}$$

Then, by the calculations for the stationary target above,

$$\begin{aligned}\dot{\Phi} &= -\frac{1}{2}\sum_{i=1}^{N}\sum_{j\neq i}^{N} f_{al}(\|\tilde{p}_{ij}\|)\|\tilde{v}_i - \tilde{v}_j\|^2 - a_v\sum_{i=1}^{N}\|\tilde{v}_i\|^2 \\ &= -\frac{1}{2}\sum_{i=1}^{N}\sum_{j\neq i}^{N} f_{al}(\|p_{ij}\|)\|v_i - v_j\|^2 - a_v\sum_{i=1}^{N}\|v_i - v_d\|^2. \end{aligned}\tag{3.8}$$

Note that $\dot{\Phi}$ is negative semidefinite and equal to zero if and only if $\tilde{v}_i = 0$ (or equivalently $v_i = v_d$) for all i, i.e., when vehicles' velocities are aligned with the velocity of the domain. The construction of this Lyapunov function leads to the following flocking result.

Theorem 3.3.1 (Flocking with the moving target)**.** *Consider a target domain Ω_t that moves with constant velocity v_d, and a group of N vehicles with smooth dynamics governed by* (3.1)*, with the control law given by* (3.2)*. Then, the group of agents has a time-asymptotic flocking with the moving target Ω_t.*

Proof. We have to check the conditions in Definition 3.1.1. For condition 1 (group cohesiveness) we will use relative coordinates $\tilde{p}_i$ and show that they remain within a compact set through time evolution. Using that the kinetic energy and the potential V_I are non-negative, and Φ given by (3.7) is non-increasing, we have:

$$\sum_{i=1}^{N} V_h\left(\tilde{p}_i(t)\right) \leq \Phi(t) \leq \Phi(0).$$

Recall that in relative coordinates the distances to the target are with respect to the fixed initial domain Ω (see (3.4)). To show boundedness of $\tilde{p}_i$ we only need to consider the case $\tilde{p}_i \notin \Omega$, or else the vehicles are inside the compact set Ω. Using the expression (2.5) for V_h, we then find:

$$\frac{a_h}{2}\sum_{i=1}^{N}\left(\|\tilde{p}_i(t) - P_{\partial\Omega}\tilde{p}_i(t)\| + \frac{r_d}{2}\right)^2 \leq \Phi(0).$$

This shows that the distances from $\tilde{p}_i(t)$ to the domain Ω remain bounded by $\sqrt{\frac{2\Phi(0)}{a_h}}$ when $\tilde{p}_i \notin \Omega$, therefore, there exists $R > 0$ such that $\|\tilde{p}_i(t)\| \leq R$, for all i and $t \geq 0$. In original variables this writes as $\|p_i(t) - p_d(t)\| \leq R$, for all i and $t \geq 0$, showing condition 1.

To show condition 2, we note that the velocities are also uniformly bounded in time. Indeed, since the potentials V_I and V_h are non-negative and Φ is non-increasing, we have:

$$\sum_{i=1}^{N} \|\tilde{v}_i(t)\|^2 \leq 2\Phi(t) \leq 2\Phi(0).$$

Hence, the solutions $(\tilde{p}_i(t), \tilde{v}_i(t))$ of the relative system are confined within a compact set through dynamics. By LaSalle Invariance Principle we can then conclude that the solutions approach asymptotically the largest invariant set in $\{\dot{\Phi} = 0\}$. Consequently, we infer from (3.8) that as $t \to \infty$, the vehicles' velocities approach the velocity of the target domain, which establishes condition 2 in Definition 3.1.1. □

Remark 3.3.2. *It has been inferred in the proof of Theorem 3.3.1 that solutions of the relative system approach asymptotically critical points of Φ that satisfy $\tilde{v}_i = 0$ for all i. By the expressions* (3.5) *of the control force and* (3.7) *of the Lyapunov function, these are equilibria that are critical points of the artificial potential energy $\sum_{i=1}^{N}\Big(\sum_{j\neq i}^{N} V_I\left(\tilde{p}_{ij}\right) + 2V_h\left(\tilde{p}_i\right)\Big)$. As also noted in the stationary case (see Remark 2.2.3), we expect that almost every solution of the relative system will approach asymptotically a local minimum of this potential energy.*

Most relevant to our study are the r_d-covers discussed in Section 2, now in the context of these configurations being equilibria in the moving frame of the target. At such relative equilibria the potential energy vanishes, as any two vehicles are more than r_d distance apart and any vehicle is at a signed distance less than $-\frac{r_d}{2}$ from Ω. Hence these equilibria in the moving frame are global minimizers of the potential energy. In certain simple geometries (e.g., a square number of vehicles in a square domain or a triangular number of vehicles in a triangular domain), such equilibria are also isolated. These observations, together with the Lyapunov function construction above and LaSalle Invariance Principe allows us to establish the following local asymptotic result.

Proposition 3.3.3. *Consider a target domain Ω_t that moves with constant velocity v_d, and a group of N vehicles with dynamics defined by* (3.1) *and* (3.2)*. Let the relative equilibrium of interest be of the form $\dot{\tilde{p}}_i = 0$, $\|\tilde{p}_{ij}\| \geq r_d$ and $[[\tilde{h}_i]] \leq -\frac{r_d}{2}$ for $i, j = 1, \cdots, N$ (see Definitions 2.1.1 and 2.1.2), and assume that this equilibrium configuration is isolated. Also assume that there is a neighborhood about the equilibrium in which the control law remains smooth. Then, the relative equilibrium is a global minimum of the sum of all the artificial potentials and is locally asymptotically stable.*

Remark 3.3.4. *All considerations in this section apply to the case of zero inter-individual alignment forces ($f_{al} = 0$). In such case, by working in the moving frame of the domain, the problem reduces in fact to the one studied in Chapter 2.*

As mentioned in Remark 2.4.1, the previous theoretical results only can be guaranteed if the control force remains sufficiently small, in other words, if it is threshold free.

3.4 Numerical simulations

In this section, we show three numerical simulation scenarios for vehicles using the coverage controller with velocity alignment we presented above. While the first two scenarios are covered by the discussed theory, the last one illustrates how our strategy still leads to appropriate final configurations even when the domain follows non-inertial trajectories. The possible safety issues are addressed as described in Section 2.3.

Triangular domain. We consider the scenario in which an equilateral triangular domain moving with constant velocity, $v_d = \left(\frac{\sqrt{2}}{2}, \frac{\sqrt{2}}{2}\right)$, is covered by a triangular number of vehicles, i.e. $N = \frac{n(n+1)}{2}$, $n \in \mathbb{N}$. At the start of the simulation the vehicles lie on a line outside the domain. The evolution for a group of $N = 10$ agents, each of them using the coverage with velocity alignment and pairwise safety strategies discussed above, is illustrated in Figures 3.1a - 3.1c. The tails represent the 15-second history of the vehicle positions.

We verified that not including the pairwise safety strategy increases the number of collisions, going from zero collision to seven when not using it. In this particular case the inclusion of the safety policy does not seem to benefit much how the system reaches the desired coverage, compare Figure 3.1b vs. Figure 3.1e.

We also want to point out some of the effects we observed when using extreme velocity alignment forces. This observations are hopefully useful while tuning parameters. Figure 3.2 shows the evolution of the vehicles when increasing the alignment constants C_{al} and a_v used in the Figure 3.1 setup from $0.2\,(\mathrm{m/s^2})$ to $1.4\,(\mathrm{m/s^2})$, while keeping the other parameters the same.

We note that strong alignments, i.e. large a_v or C_{al} values, may cause that the vehicles spread slowly inside the domain, compare Figures 3.2a and 3.2b vs. Figure 3.1e. In addition, very strong velocity alignments can make the systems more prone to not reaching the desired formations.

On the other hand, weak alignments, i.e. small a_v and C_{al} values, cause undesired overshoots, and slower asymptotic flocking. Therefore, it is important to maintain a good balance between the strength of the alignment and coverage forces.

Non-convex domain. We now study the scenario in which vehicles cover and follow a non-convex moving domain. While the domain preserves its shape, it moves with a constant velocity $v_d = \left(\frac{\sqrt{2}}{2}, \frac{\sqrt{2}}{2}\right)$. Different time instants of the simulation are shown in Figure 3.3, where the tails represent the vehicle positions during the last 20 seconds of the simulation.

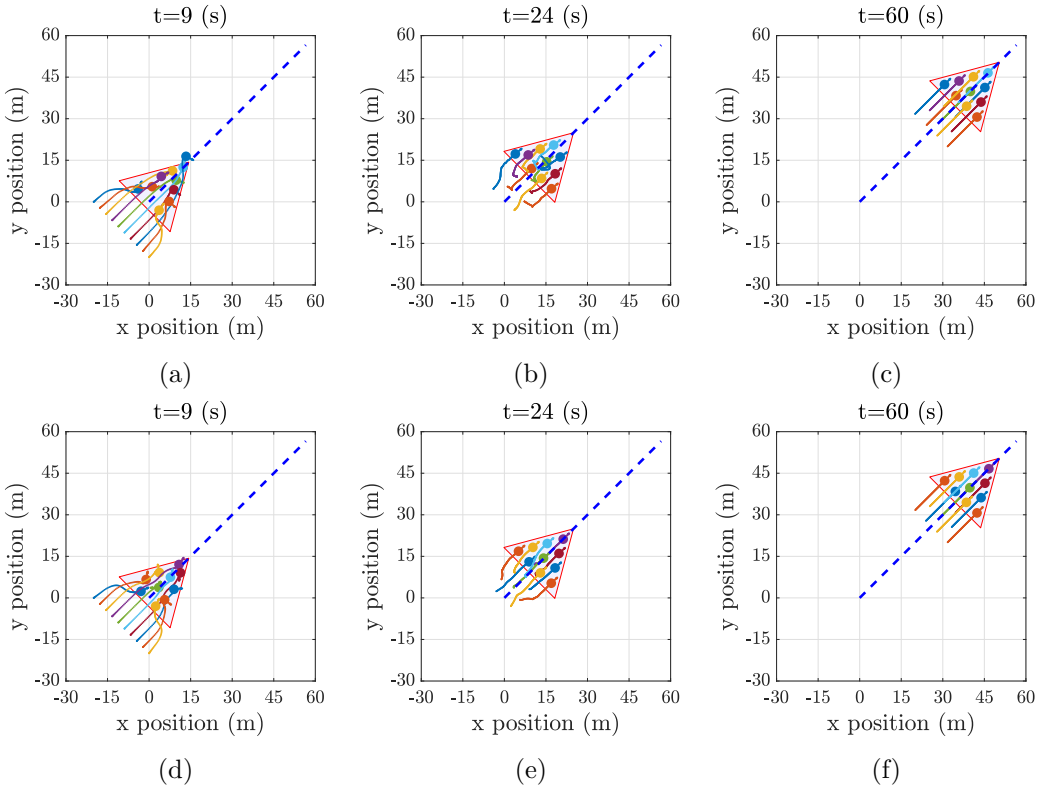

Figure 3.1: Vehicles covering and following a moving equilateral triangular domain, when $N = 10$, $c_r = 2\,(\mathrm{m})$, $v_{max} = 10\,(\mathrm{m/s})$, $u_{max} = 3\,(\mathrm{m/s^2})$, $t_{safety} = 5\,(\mathrm{s})$, $a_I = 1\,(\mathrm{m/s^2})$, $a_h = 2\,(\mathrm{m/s^2})$, $a_v = 0.2\,(\mathrm{m/s^2})$, $C_{al} = 0.2\,(\mathrm{m/s^2})$, $l_{al} = 7.79\,(\mathrm{m})$, $v_d = \left(\frac{\sqrt{2}}{2}, \frac{\sqrt{2}}{2}\right)\,(\mathrm{m/s})$, domain area $A = 292.28\,(\mathrm{m^2})$ and $r_d = \sqrt{\frac{A}{N}} = 5.4\,(\mathrm{m})$. Vehicles start in linear formation. (a)-(c) include collision avoidance controller, (d)-(f) do not.

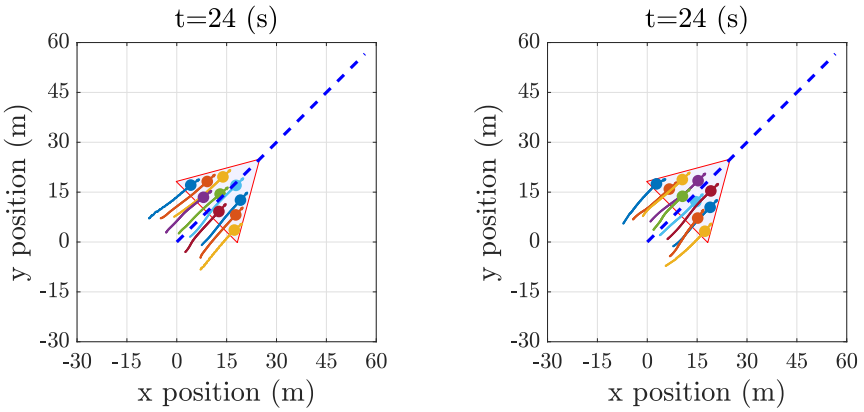

(a) $C_{al} = 0.2\,(\mathrm{m/s^2})$, $a_v = 1.4\,(\mathrm{m/s^2})$ (b) $C_{al} = 1.4\,(\mathrm{m/s^2})$, $a_v = 0.2\,(\mathrm{m/s^2})$

Figure 3.2: Effects of strong velocity alignment for vehicles covering a moving equilateral triangular domain, when $N = 10$, $c_r = 2\,(\mathrm{m})$, $v_{max} = 10\,(\mathrm{m/s})$, $u_{max} = 3\,(\mathrm{m/s^2})$, $t_{safety} = 5\,(\mathrm{s})$, $a_I = 1\,(\mathrm{m/s^2})$, $a_h = 2\,(\mathrm{m/s^2})$, $l_{al} = 7.79\,(\mathrm{m})$, $v_d = \left(\frac{\sqrt{2}}{2}, \frac{\sqrt{2}}{2}\right)$ (m/s), domain area $A = 292.28\,(\mathrm{m^2})$ and $r_d = \sqrt{\frac{A}{N}} = 5.4\,(\mathrm{m})$. Vehicles start in linear formation and do not include collision avoidance controller.

Initially, all the 9 vehicles lie on a line perpendicular to the movement direction of the target domain, as shown by the tails of the vehicles in Figure 3.3a.

We distinguish two main behaviours: during a first phase of the simulation (Figures 3.3a and 3.3b) the vehicles cover the domain approximately evenly, adopting the arrow shape, while in a second phase (Figure 3.3c), a clearer domain-following behaviour is observed. The oscillations of the two vehicles that are lagging behind are the effect of their proximity to the corners. Indeed, as one of the line segments of the boundary wedge gets closer to the vehicle near the corner, it pushes it towards the other segment of the wedge, a back-and-forth motion that causes the zigzagging. These oscillations can be reduced by reinforcing the velocity alignment.

Unlike the convex case, in non-convex domains the projection on the boundary for points outside of the domain may not be unique; this is the case for instance of the green vehicle in the middle of the initial setup – see start of the tails in Figure 3.3a. Although the chance for a vehicle to lie in one of these states is extremely unlikely (the set of points where this happens has zero measure), this fact may yield ambiguity in the definition of the domain-vehicle force. We mitigate this issue by considering the contribution from only one of the multiple projection points; consequently, the numerical time evolution may depend on the chosen projection method.

Domain Moving in a Circle. Finally, we include the case of a target domain moving with non-zero acceleration, more specifically, an equilateral triangular domain under translation and rotation. While the translation of its centre of mass describes a circular motion of

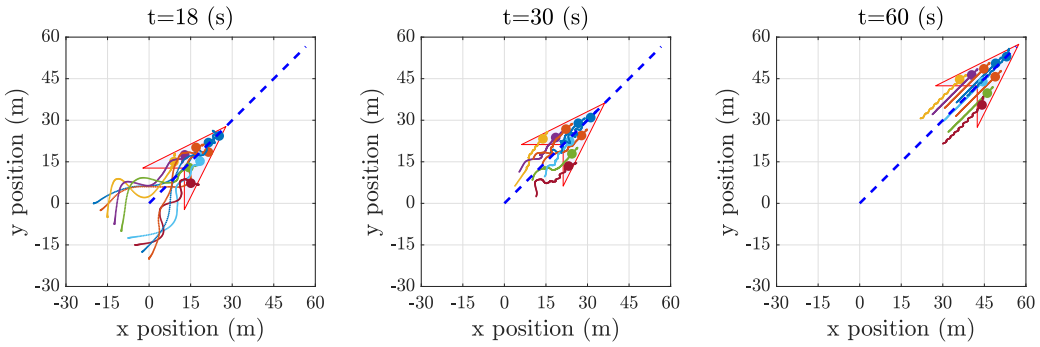

(a) (b) (c)

Figure 3.3: Vehicles covering and following a moving, non-convex domain, when $N = 9$, $c_r = 2\,(\mathrm{m})$, $v_{max} = 10\,(\mathrm{m/s})$, $u_{max} = 3\,(\mathrm{m/s^2})$, $t_{safety} = 5\,(\mathrm{s})$, $a_I = 1\,(\mathrm{m/s^2})$, $a_h = 2\,(\mathrm{m/s^2})$, $a_v = 0.2\,(\mathrm{m/s^2})$, $C_{al} = 0.1\,(\mathrm{m/s^2})$, $l_{al} = 7.21\,(\mathrm{m})$, domain area $A = 225\,(\mathrm{m^2})$ and $r_d = \sqrt{\frac{A}{N}} = 5\,(\mathrm{m})$. The vehicles start in linear formation, approach and cover the domain, while following it. The vehicles lagging behind exhibit oscillations due to a bouncing effect in the narrow corners.

radius 30 with constant angular velocity $\frac{2\pi}{40}$, the rotation aligns the heading of the half line to be tangent to that circle, see Figure 3.4. Note that this non-inertial path plus rotation is not covered by our previous theoretical results (Theorem 3.3.1 and Proposition 3.3.3).

The vehicles' time evolution is illustrated in Figure 3.4, where the tails represent the vehicles position during the last 20 seconds of the simulation. At the beginning, the $N = 6$ vehicles are in the line formation as shown by the beginning of the tails in Figure 3.4a. As in previous simulations the vehicles try to reach the moving domain, this time rotating around the domain circular path (Figures 3.4a and 3.4b). Then, the vehicles reach coverage of the domain (Figure 3.4c) which is maintained by each vehicle by remaining in a circular movement of constant radius (Figure 3.4d).

When a vehicle describes a uniform circular movement with angular velocity ω and radius r, its speed remains constant over time and is given by $r\omega$. Now, as the vehicles move asymptotically along circles with different radii, we can conclude they have different velocities, it means this type of "flock" does not satisfy Def. 3.1.1. In contrast to the case when the domain is moving along inertial paths, in this case each vehicle's control force magnitude does not go asymptotically to zero, but instead, it tends to approach its centripetal acceleration $r\omega^2$.

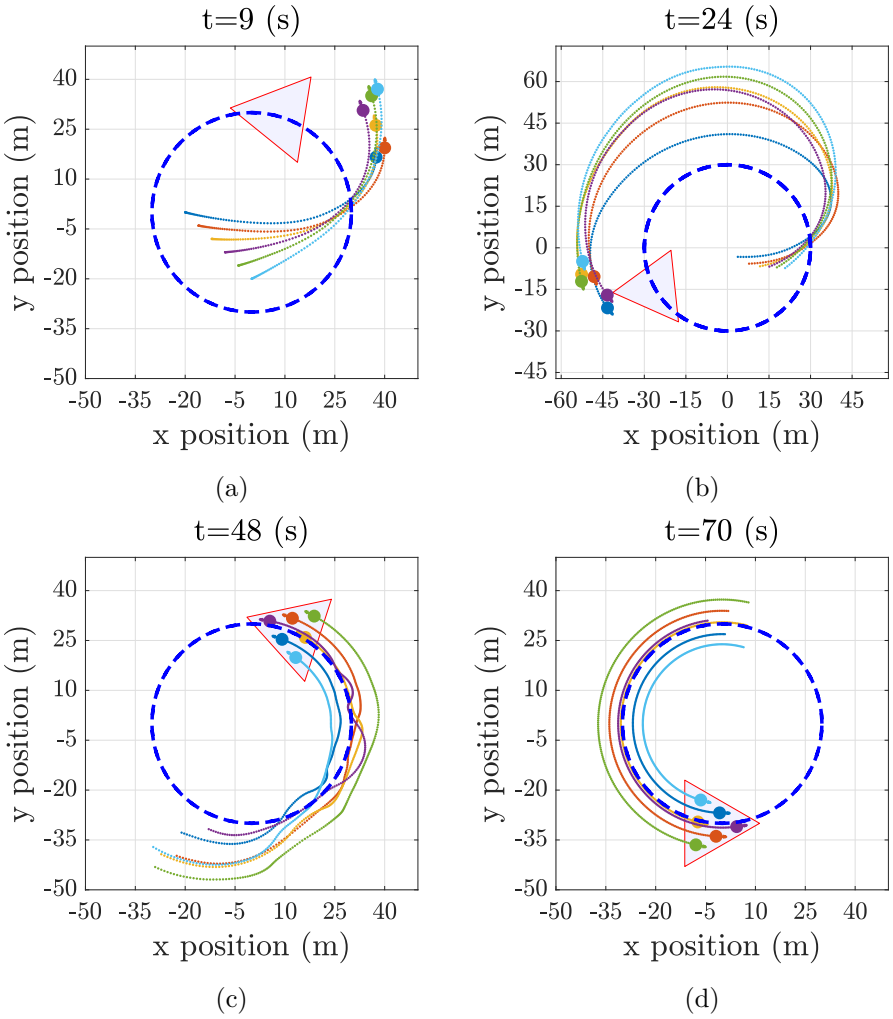

Figure 3.4: Vehicles covering and following a non-zero acceleration triangular domain moving over the path $\left(30\cos\left(\frac{2\pi}{40}t\right), 30\sin\left(\frac{2\pi}{40}t\right)\right)$, when $N = 6$, $c_r = 2\,(\mathrm{m})$, $v_{max} = 10\,(\mathrm{m/s})$, $u_{max} = 3\,(\mathrm{m/s^2})$, $t_{safety} = 5\,(\mathrm{s})$, $a_I = 10\,(\mathrm{m/s^2})$, $a_h = 10\,(\mathrm{m/s^2})$, $a_v = 1\,(\mathrm{m/s^2})$, $C_{al} = 1.2\,(\mathrm{m/s^2})$, $l_{al} = 10.06\,(\mathrm{m})$, domain area $A = 292.28\,(\mathrm{m^2})$ and $r_d = \sqrt{\frac{A}{N}} = 6.97\,(\mathrm{m})$. The vehicles start in linear formation, approach and cover the domain, while following it.

Chapter 4

Planar Fixed-Wing Aircraft

4.1 Problem Formulation

In this chapter consider again the flocking coverage problem where the target domain moves with prescribed constant velocity v_d (see Definitions 2.1.1, 2.1.2 and 3.1.1). The difference here is that instead of following the 2nd-order dynamics (3.1) each of the N vehicles is governed by the planar fixed-wing aircraft dynamics

$$\begin{gathered} \dot{p_i} = s_i \left(\cos\left(\theta_i\right), \sin\left(\theta_i\right)\right), \ \left(\dot{\theta}_i, \dot{s}_i\right) = \left(u_{i,\theta}, u_{i,s}\right); \\ 0 < s_{min} \leq \|\dot{p_i}\| \leq s_{max}, \ |u_{i,\theta}| \leq u_{\theta_{max}}, \ |u_{i,s}| \leq u_{s_{max}}. \end{gathered} \tag{4.1}$$

Here, θ_i is the heading angle, s_i is the vehicle speed and $p_i = (p_{i,x}, p_{i,y})$ is the position of the i-th agent. The variables $u_{i,s}$ and $u_{i,\theta}$ are the acceleration and turn rate applied to this vehicle respectively; these are the control inputs to be specified later. In addition to the bounds for the controls, we also impose maximum and minimum speed limits, the last being particularly relevant for aerial vehicles.

In this case, our safe domain coverage problem of interest is the following:

Safe-domain-coverage for moving domain by planar fixed-wing air-crafts: *Consider a compact domain Ω_t that moves with constant velocity v_d in the plane, and N vehicles with dynamics described by* (4.1)*, starting from safe initial conditions. Find the maximal $r > 0$ and a control policy that leads to an r-cover for Ω_t that flocks with the moving target, while satisfying the safety condition* (2.2) *at any time.*

4.2 Coverage Controller

Our purpose is to find expressions for each agent's control law based on the proposed coverage policy with inter-vehicle and vehicle-domain alignment forces (3.2), while satisfying the constraints given in (4.1).

By differentiation of the vehicle dynamics (4.1) with respect to time, one can find that the acceleration in Cartesian coordinates of the i-th agent in terms of the control inputs are as follows:

$$\begin{pmatrix} \ddot{p}_{i,x} \\ \ddot{p}_{i,y} \end{pmatrix} = R(\theta_i, s_i) \begin{pmatrix} u_{i,\theta} \\ u_{i,s} \end{pmatrix}; \text{ where } R(\theta_i, s_i) := \begin{pmatrix} -s_i \sin(\theta_i) & \cos(\theta_i) \\ s_i \cos(\theta_i) & \sin(\theta_i) \end{pmatrix}. \tag{4.2}$$

This relation allows us to compute an expression for the vehicle control inputs in terms of its acceleration in Cartesian coordinates whenever $s_i \neq 0$ as

$$\begin{pmatrix} u_{i,\theta} \\ u_{i,s} \end{pmatrix} = (R(\theta_i, s_i))^{-1} \begin{pmatrix} \ddot{p}_{i,x} \\ \ddot{p}_{i,y} \end{pmatrix}. \tag{4.3}$$

Using this correspondence, one can obtain the necessary controls $(u_{i,\theta}, u_{i,s})$ to achieve the same acceleration in Cartesian coordinates produced by the proposed control force (3.2) as

$$\begin{pmatrix} u_{i,\theta} \\ u_{i,s} \end{pmatrix} = (R(\theta_i, s_i))^{-1} \left(-\sum_{j \neq i}^{N} f_I(\|p_{ij}\|) \frac{p_{ij}}{\|p_{ij}\|} - f_h([[h_i]]) \frac{h_i}{[[h_i]]} - \sum_{j \neq i}^{N} f_{al}(\|p_{ij}\|) v_{ij} - a(v_i - v_d) \right). \tag{4.4}$$

The changes of coordinates (4.2) and (4.3) guarantee that all the stability results in Chapter 3 are still valid in the case of the planar fixed-wing aircraft model when no constraints are applied as long as none of the vehicles stop along their trajectories. This seems to be a very plausible assumption in practice as the minimum speed is supposed to be greater than zero.

Thresholding the Control Force While finding an admissible force satisfying the constraints for the double integrator model (3.1) is done by simply normalizing the vehicles control input (3.2), obtaining a suitable fixed-wing control input satisfying the constraints (4.1) is not as straightforward.

In order to obtain the appropriate planar fixed-wing aircraft control inputs we use the relation (4.2), which allow us to represent the set of admissible accelerations from the Cartesian perspective as

$$S(\theta_i, s_i) = \left\{ R(\theta_i, s_i) \begin{pmatrix} u_\theta \\ u_s \end{pmatrix} : \begin{pmatrix} u_\theta \\ u_s \end{pmatrix} \in [-u_{\theta_{max}}, u_{\theta_{max}}] \times [-u_{s_{max}}, u_{s_{max}}] \right\}.$$

This set can be understood as a stretch and rotation of the rectangle containing the admissible vehicle control inputs.

The input constraints certainly affect the magnitude of the vehicle acceleration, however, we intend to preserve its direction. Let us define the Cartesian admissible force associated

to the control (4.4) as

$$\begin{pmatrix} \hat{u}_{i,x} \\ \hat{u}_{i,y} \end{pmatrix} = \sup \left\{ t \in \mathbb{R} : tR\left(\theta_i, s_i\right) \begin{pmatrix} u_{i,\theta} \\ u_{i,s} \end{pmatrix} \in S\left(\theta_i, s_i\right) \right\} R\left(\theta_i, s_i\right) \begin{pmatrix} u_{i,\theta} \\ u_{i,s} \end{pmatrix},$$

i.e. the largest acceleration in the set of admissible accelerations in Cartesian coordinates that is parallel to the desired acceleration, see Figure 4.1.

Finally, the thresholded fixed-wing aircraft control inputs can be obtained by using the relation (4.2) as

$$\begin{pmatrix} \hat{u}_{i,\theta} \\ \hat{u}_{i,s} \end{pmatrix} = \left(R\left(\theta_i, s_i\right)\right)^{-1} \begin{pmatrix} \hat{u}_{i,x} \\ \hat{u}_{i,y} \end{pmatrix},$$

or simply,

$$\begin{pmatrix} \hat{u}_{i,\theta} \\ \hat{u}_{i,s} \end{pmatrix} = \sup \left\{ t \in \mathbb{R} : tR\left(\theta_i, s_i\right) \begin{pmatrix} u_{i,\theta} \\ u_{i,s} \end{pmatrix} \in S\left(\theta_i, s_i\right) \right\} \begin{pmatrix} u_{i,\theta} \\ u_{i,s} \end{pmatrix}.$$

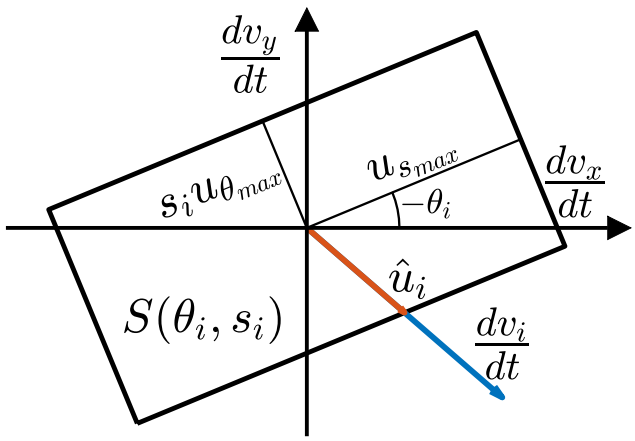

Figure 4.1: Thresholded fixed-wing aircraft control input $\hat{u}_i$ for vehicle with speed s_i and heading θ_i computed from its set of admissible accelerations in Cartesian coordinates $S\left(\theta_i, s_i\right)$ and a reference acceleration $\frac{dv_i}{dt}$.

Some comments on collision avoidance. As mentioned above, the changes of coordinates (4.2) and (4.3) guarantee that the unconstrained fixed-wing aircraft dynamics satisfy the vehicles safety conditions when the initial energy is small enough, as established in Proposition 2.3.1.

On the other hand, as the set of control inputs and non-anticipative disturbances differ from those in the double integrator dynamics, the collision avoidance via Hamilton-Jacobi reachability for this type of vehicle requires a different study than the one carried out in Section 2.3. Obtaining an analytical solution for the HJ PDE associated is much more difficult and solving it numerically is computationally challenging. As it requires more attention, we decide to exclude the collision avoidance controller in the following numerical simulations, and consider it as part of our future work.

4.3 Numerical Simulations

In this section we revisit the simulation scenarios investigated in Section 3.4 and illustrate how our control strategy leads to similar coverage configurations. We do not intend to compare the systems evolution, as they are two distinct types of vehicles with different capabilities. ,

Triangular domain. In the first scenario, we consider an equilateral triangular domain moving with constant velocity, $v_d = \left(\frac{\sqrt{2}}{2}, \frac{\sqrt{2}}{2}\right)$, which is covered by a triangular number of vehicles. The minimum for vehicle's speed is set at $0.5\,(\mathrm{m/s})$, while the maximum is $10\,(\mathrm{m/s})$. Each of the fixed-wing agents uses the coverage controller with velocity alignment (4.4) discussed in Section 4.2.

Figure 4.2 shows three different time steps of the evolution of the vehicles. The tails represent the last 15 seconds of the vehicles position history. At the start of the simulation the $N = 10$ vehicles lie on a line outside the domain moving with the minimum allowed speed and random headings, see Figure 4.2a.

At time $t = 0\,(\mathrm{s})$ the major acceleration effects are associated to the vehicle-domain forces, which pull the agents to the domain. This causes that the vehicles not pointing towards the domain accelerate less and lag with respect to the others, see Figure 4.2b. The reason for this is that for low speed vehicles the threshold is more restrictive when the acceleration direction does not agree with the movement direction, as illustrated by Figure 4.1.

As time goes on, the vehicles approach the domain (Figures 4.2b and 4.2c), and then cover it by taking a triangular formation moving with constant velocity as expected, see Figures 4.2d and 4.2e. In this particular case, the same coverage controller parameters used for the double integrator vehicles seem to work well. However, it is not a rule of thumb, as the thresholding strategies are very different.

We consider it remarkable that the system does not present collisions despite not having any safety-oriented system. It suggests that the combination of inter-vehicle spatial and alignment forces may be enough to guarantee safety under certain conditions, even when thresholding the control inputs.

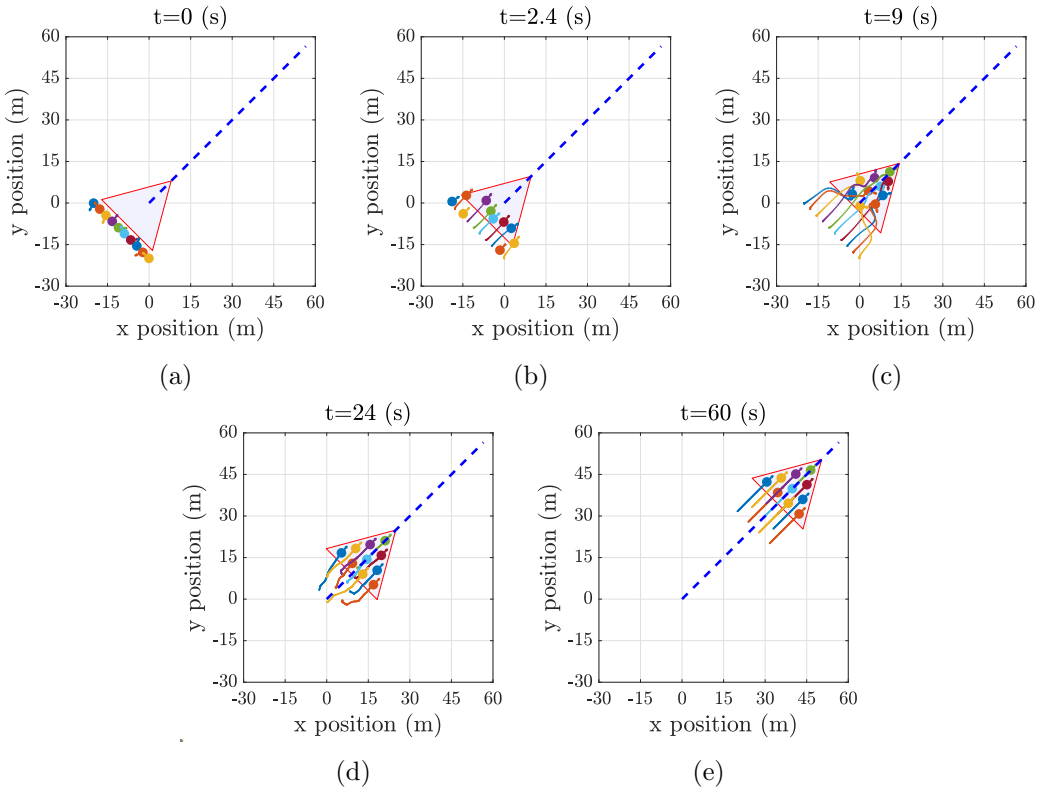

Figure 4.2: Vehicles with planar fixed-wing aircraft dynamics covering and following a moving equilateral triangular domain, when $N = 10$, $c_r = 2\,(\mathrm{m})$, $s_{max} = 10\,(\mathrm{m/s})$, $s_{min} = 0.5\,(\mathrm{m/s})$, $u_{\theta_{max}} = \pi/2\,(\mathrm{rad/s})$, $u_{s_{max}} = 3\,(\mathrm{m/s^2})$, $a_I = 1\,(\mathrm{m/s^2})$, $a_h = 2\,(\mathrm{m/s^2})$, $a_v = 0.2\,(\mathrm{m/s^2})$, $C_{al} = 0.2\,(\mathrm{m/s^2})$, $l_{al} = 7.79\,(\mathrm{m})$, $v_d = \left(\frac{\sqrt{2}}{2}, \frac{\sqrt{2}}{2}\right)\,(\mathrm{m/s})$, domain area $A = 292.28\,(\mathrm{m^2})$ and $r_d = \sqrt{\frac{A}{N}} = 5.4\,(\mathrm{m})$. Collision avoidance controller is not included. The vehicles start in linear formation.

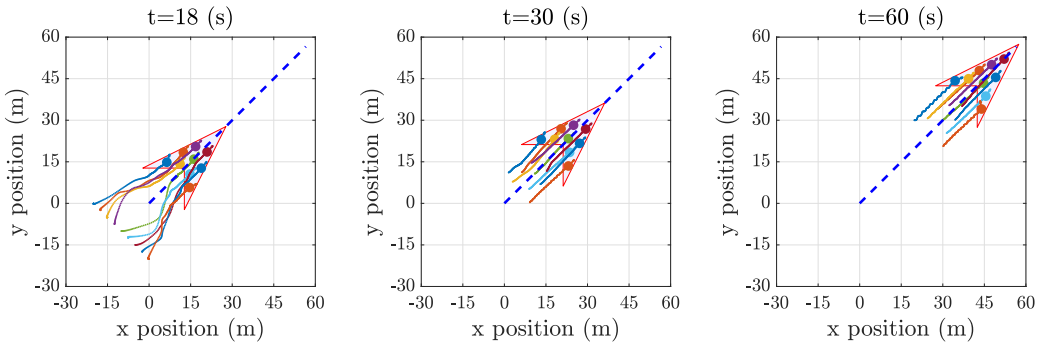

(a) (b) (c)

Figure 4.3: Nine vehicles with planar fixed-wing aircraft dynamics covering and following a moving, non-convex domain, $c_r = 2\,(\mathrm{m})$, $s_{max} = 10\,(\mathrm{m/s})$, $s_{min} = 0.5\,(\mathrm{m/s})$, $u_{\theta_{max}} = \pi/2\,(\mathrm{m/s^2})$, $u_{s_{max}} = 3\,(\mathrm{m/s^2})$, $a_I = 5\,(\mathrm{m/s^2})$, $a_h = 2\,(\mathrm{m/s^2})$, $a_v = 0.2\,(\mathrm{m/s^2})$, $C_{al} = 2\,(\mathrm{m/s^2})$, $l_{al} = 7.21\,(\mathrm{m})$, domain area $A = 225\,(\mathrm{m^2})$ and $r_d = \sqrt{\frac{A}{N}} = 5\,(\mathrm{m})$. The vehicles start in linear formation, approach and cover the domain, while following it. The collision avoidance controller is not included. The vehicles lagging behind exhibit oscillations due to a bouncing effect in the narrow corners.

Non-convex domain. In the second scenario a group of vehicles cover and follow a non-convex domain moving with constant velocity $v_d = \left(\frac{\sqrt{2}}{2}, \frac{\sqrt{2}}{2}\right)$. As above, the minimum vehicle speed is set at $0.5\,(\mathrm{m/s})$ and the maximum at $10\,(\mathrm{m/s})$. Different time instants of the simulation are shown in Figure 4.3, where the tails represent the last 20 seconds of the vehicles position history. Initially, all the 9 fixed-wing agents lie on a line perpendicular to the movement direction of the target domain, as shown by the tails of the vehicles in Figure 4.3a.

We can distinguish again the follow-cover (Figures 4.3a and 4.3b) and the flocking around the domain (Figure 4.3c) behaviours. Similarly, we observe the oscillations of the two vehicles that are lagging behind, due to their proximity to the corners.

When we use the same coverage controller parameters as in the double integrator scenario, there are many collisions. In order to obtain a free collision movement we use two strategies. On the one hand, we increase the inter-vehicle non-zero slope, a_I, to promote vehicles to stay apart. On the other hand, we increase the inter-vehicle velocity alignment strength, C_{al}, which prevents nearby vehicles to move directly towards each other. Finally, note that the agents slow down the spread inside the domain due to the strong velocity alignment (Figure 4.3b).

Domain Moving in a Circle. Finally, we present the accelerated domain case, where $N = 6$ vehicles cover an equilateral triangle whose center of mass follows an uniform circular motion of radius 30 an angular velocity $\frac{2\pi}{40}$ while rotates to align the half line heading to be tangent to the circle described, see Figure 4.4. The agents time evolution is illustrated

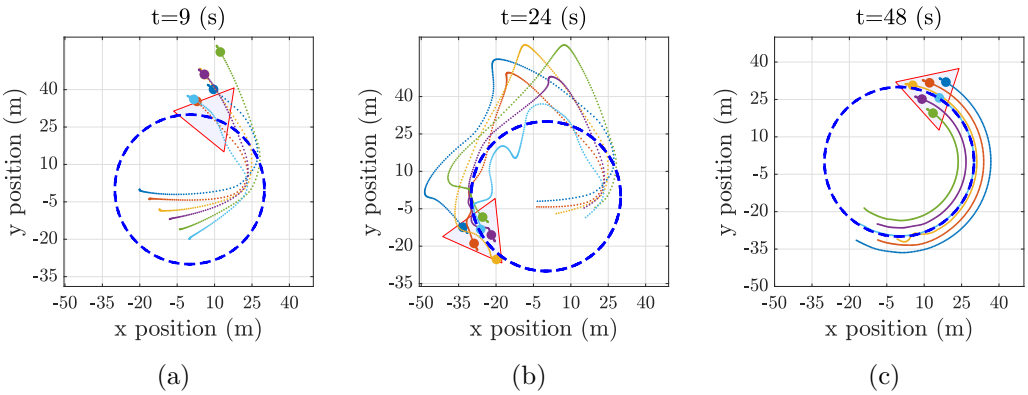

(a) (b) (c)

Figure 4.4: Vehicles with planar fixed-wing aircraft dynamics covering and following a non-zero acceleration triangular domain moving over the path $\left(30\cos\left(\frac{2\pi}{40}t\right), 30\sin\left(\frac{2\pi}{40}t\right)\right)$, when $N = 6$, $c_r = 2\,(\text{m})$, $s_{min} = 0.5\,(\text{m/s})$, $s_{max} = 10\,(\text{m/s})$, $u_{\theta max} = \pi/2\,(\text{rad/s})$, $u_{smax} = 3\,(\text{m/s}^2)$, $a_v = 1.2$, $l_{al} = 3.679$, $C_{al} = 1.5$, $a_I = 5$, $a_h = 2.7$, domain area $A = 292.28\,(\text{m}^2)$ and $r_d = \sqrt{\frac{A}{N}} = 6.97\,(\text{m})$. The vehicles start in a linear formation, approach and cover the domain, while following it. The collision avoidance controller is not included.

in Figure 4.4, where the tails represent the vehicles position during the last 20 seconds of the simulation.

The vehicles start in a line formation shown by the tails in Figure 4.4. They reach the target domain and spread inside of it (Figures 4.4a and 4.4b). Once they cover the domain, each of the fixed-wing agents follows a circular path of radius r and constant angular velocity $\omega = \frac{2\pi}{40}$ (Figure 4.4c). Under this configuration the vehicles have reached their terminal speed $r\omega$ and do not require extra acceleration, i.e. $u_s = 0$, however they should maintain a turn rate of $u_\theta = \omega$.

Chapter 5

Conclusion

5.1 Summary of Results

We proposed a method for multi-vehicle coordination which allows a swarm of vehicles to cover moving compact planar shapes. Vehicles are modeled using two different second-order dynamics (double integrator and planar fixed-wing aircraft) with bounded control inputs, which is more realistic than the first-order models commonly used for coverage problems.

Coverage by vehicles with double integrator dynamics. The coverage controller for vehicles with double integrator dynamics is based on artificial potentials and consensus forces among vehicles, and between each vehicle and the moving domain of interest. The safety controller is based on Hamilton-Jacobi reachability, which guarantees pairwise collision avoidance. Besides drastically reducing collision count, the safety controller also helps break symmetries and lead to faster convergence to steady states.

Under the proposed control law we proved that: i) the vehicles remain cohesive around the domain, Proposition 2.2.2, ii) the cover configurations of interest are locally stable equilibrium points, Propositions 2.2.4 and 3.3.3, and (iii) the agents flock with the target, Theorem 3.3.1. Regarding collision avoidance, we show that for small initial energy configurations the non-thresholded control guarantees a collision free movement in the case of inertial moving domains, Propositions 2.3.1 and 2.3.2. We also found an analytical closed expression for the coverage controller based on HJ pairwise avoidance, Proposition 2.3.3.

Coverage by vehicles with planar fixed-wing aircraft dynamics. The control law for vehicles with planar fixed-wing aircraft dynamics uses a transformation and tresholding mechanism of the double integrator coverage control policy. The collision avoidance for this type of vehicle was not implemented as the associated HJ-PDE is numerically challenging, see future work for some more details.

Numerical simulations. We demonstrate the successful results of our coverage approach for static and moving domains on four representative simulations scenarios involving: a

static square and non-accelerated moving triangular and non-convex domains, in addition to a triangular domain following a circular path. While the first three scenarios are covered by our theoretical results the latter is not, however, it shows satisfactory results, suggesting some generality of the proposed technique.

5.2 Future Work

Immediate future work includes parameter tuning to reduce oscillations in the vehicles' movement, studying three-dimensional coverage, investigating geometrical properties of steady states, investigating scenarios involving partial information, and implementing our approach on robotic platforms.

Fixed-Wing Aircraft Pairwise Collision Avoidance

As mentioned in Chapter 4, the pairwise collision avoidance for the planar fixed-wing aircraft type of vehicle requires a different analysis than the carried out in Section 2.3 and it was not done as part of this thesis. We introduce here briefly the problem to resolve.

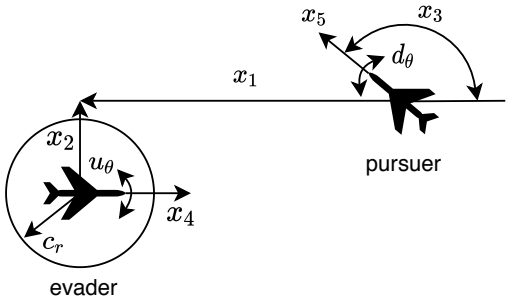

Figure 5.1: Relative coordinate system for pairwise collision avoidance in the fixed-wing scenario. Figure adapted with the permission of authors from [35] © [2005] IEEE.

As done in the double integrator case, we should consider the relative dynamics between a pair of vehicles, where one acts as evader and the other as pursuer. Using as reference the Figure 5.1, to obtain the relative dynamics we consider the evader fixed at the origin facing the positive x_1 axis. Here x_1 is the projection of the vector connecting the vehicle's positions on the axis parallel to the evader's heading, and x_2 is its projection on the orthogonal direction, x_3 represents the difference of the two agents headings while x_4 and x_5 represent the evader and pursuer speeds respectively. The pursuer's speed, relative location and heading as well as the evader's speed are described by the following dynamical system

$$\dot{x} = f(x, u, d) = \begin{pmatrix} x_5 \cos(x_3) - x_4 + u_\theta x_2 \\ x_5 \sin(x_3) - u_\theta x_1 \\ d_\theta - u_\theta \\ u_v \\ d_v \end{pmatrix}.$$

Here $u := (u_\theta, u_s)$ and $d := (d_\theta, d_s)$, where u_θ and u_s are the evader's turn rate and acceleration, and d_θ, d_s the pursuer's ones and are treated as disturbances.

Applying the dynamic programming principle, we can obtain the time to reach ϕ as the viscosity solution for the stationary HJ PDE:

$$\begin{aligned} \min_{u \in \mathcal{U}} \max_{d \in \mathcal{D}} \{-\nabla \phi(z) \cdot f(z, u, d) - 1\} = 0, \quad & \text{in } \mathcal{R}^* \backslash \Gamma \\ \phi(x) = 0, \quad & \text{on } \Gamma, \end{aligned} \tag{5.1}$$

here $\Gamma = \{z : z_1^2 + z_2^2 \leq c_r^2\}$ is now a five dimensional cylinder on the first two dimensions of radius c_r.

The challenges of solving numerically the HJ PDE (5.1) are two-fold. First, the memory requirements to store the solution are large even for coarse resolutions, and second, the computational time scale poorly as the grid size grows. This is particularly problematic when the algorithm specifications are not optimized for the hardware architecture. In the last regard, optimized_dp is a python toolbox for solving HJ PDEs which decouples the algorithm from the hardware specifications obtaining faster executions. On the other hand, as the numerical solution is stored in a five dimensional array, obtaining the adequate resolution may require many gigabytes of RAM memory. We expect to alleviate this challenge using the new toolbox in `https://github.com/SFU-MARS/optimized_dp` to incorporate this analysis in our numerical simulations.

Bibliography

[1] Anayo K. Akametalu, Claire J. Tomlin, and Mo Chen. Reachability-Based Forced Landing System. *Journal of Guidance, Control, and Dynamics*, 41(12):2529–2542, Dec. 2018.

[2] Matthias Althoff and John M. Dolan. Set-based computation of vehicle behaviors for the online verification of autonomous vehicles. In *Proc. IEEE Int. Conf. on Intelligent Transportation Systems*, 2011.

[3] Martino Bardi. A boundary value problem for the minimum-time function. *SIAM journal on control and optimization*, 27(4):776–785, 1989.

[4] Martino Bardi and Italo Capuzzo-Dolcetta. *Optimal control and viscosity solutions of Hamilton-Jacobi-Bellman equations*. Springer Science & Business Media, 2008.

[5] S. Camazine, J-L. Deneubourg, N.R. Franks, J. Sneyd, G. Theraulaz, and E. Bonabeau. *Self-organization in biological systems*. Princeton Studies in Complexity. Princeton University Press, Princeton, NJ, 2003. Reprint of the 2001 original.

[6] Y. Cao, W. Ren, and M. Egerstedt. Distributed containment control with multiple stationary or dynamic leaders in fixed and switching directed networks. *Automatica*, 48:1586–1597, 2012.

[7] José A Carrillo, Massimo Fornasier, Giuseppe Toscani, and Francesco Vecil. Particle, kinetic, and hydrodynamic models of swarming. In *Mathematical modeling of collective behavior in socio-economic and life sciences*, pages 297–336. Springer, 2010.

[8] Juan Chacon, Mo Chen, and Razvan C Fetecau. Safe coverage of compact domains for second order dynamical systems. *To be published on IFAC 2020 Germany proceedings, preprint arXiv:1911.06519*, 2019.

[9] Mo Chen, Somil Bansal, Jaime F. Fisac, and Claire J. Tomlin. Robust Sequential Trajectory Planning Under Disturbances and Adversarial Intruder. *IEEE Trans. Control Systems Technology*, pages 1–17, Nov. 2018.

[10] Mo Chen, Jennifer C. Shih, and Claire J. Tomlin. Multi-vehicle collision avoidance via Hamilton-Jacobi reachability and mixed integer programming. In *Proc. IEEE Conf. Decision and Control*, Dec. 2016.

[11] Mo Chen and Claire J. Tomlin. Hamilton–Jacobi Reachability: Some Recent Theoretical Advances and Applications in Unmanned Airspace Management. *Annual Review of Control, Robotics, and Autonomous Systems*, 1(1):333–358, May 2018.

[12] Xin Chen, Erika Ábrahám, and Sriram Sankaranarayanan. Flow*: An Analyzer for Non-linear Hybrid Systems. In *Proc. Int. Conf. Computer Aided Verification*, 2013.

[13] S-J. Chung, A.A. Paranjape, P. Dames, S. Shen, and V. Kumar. A survey on aerial swarm robotics. *IEEE Trans. Robotics*, 34(4):837–855, 2018.

[14] J. Cortés, S. Martínez, T. Karatas, and F. Bullo. Coverage control for mobile sensing networks. *IEEE Trans. Robotics and Automation*, 20:243–255, 2004.

[15] I.D. Couzin, J. Krause, R. James, G.D. Ruxton, and N.R. Franks. Collective memory and spatial sorting in animal groups. *J. Theor. Biol.*, 218:1–11, 2002.

[16] F. Cucker and S. Smale. Emergent behavior in flocks. *IEEE Trans. Automat. Control*, 52(5):852–862, 2007.

[17] Felipe Cucker and Jiu-Gang Dong. Avoiding collisions in flocks. *IEEE Transactions on Automatic Control*, 55(5):1238–1243, 2010.

[18] M.C. Delfour and J.-P. Zolésio. *Shapes and geometries: analysis, differential calculus, and optimization*. Advances in Design and Control. SIAM, Philadelphia, PA, USA, 2001.

[19] M.R. D'Orsogna, Y-L. Chuang, A.L. Bertozzi, and L. Chayes. Self-propelled particles with soft-core interactions: patterns, stability, and collapse. *Phys. Rev. Lett.*, 96(10):104302, 2006.

[20] Joep HM Evers, Razvan C Fetecau, and Lenya Ryzhik. Anisotropic interactions in a first-order aggregation model. *Nonlinearity*, 28(8):2847, 2015.

[21] R.C. Fetecau and A. Guo. A mathematical model for flight guidance in honeybee swarms. *Bull. Math. Biol.*, 74(11):2600–2621, 2012.

[22] Goran Frehse, Colas Le Guernic, Alexandre Donzé, Scott Cotton, Rajarshi Ray, Olivier Lebeltel, Rodolfo Ripado, Antoine Girard, Thao Dang, and Oded Maler. SpaceEx: Scalable Verification of Hybrid Systems. In *Proc. Int. Conf. Computer Aided Verification*, 2011.

[23] C. Gao, J. Cortés, and F. Bullo. Notes on averaging over acyclic digraphs and discrete coverage control. *Automatica*, 44:2120–2127, 2012.

[24] Ather Gattami, Assad Al Alam, Karl Henrik Johansson, and Claire J Tomlin. Establishing Safety for Heavy Duty Vehicle Platooning: A Game Theoretical Approach. *IFAC Proceedings Volumes*, 44(1):3818–3823, Jan. 2011.

[25] Seung-Yeal Ha, Zhuchun Li, Marshall Slemrod, and Xiaoping Xue. Flocking behavior of the Cucker-Smale model under rooted leadership in a large coupling limit. *Quarterly of Applied Mathematics*, pages 689–701, 2014.

[26] Seung-Yeal Ha and Jian-Guo Liu. A simple proof of the Cucker-Smale flocking dynamics and mean-field limit. *Communications in Mathematical Sciences*, 7(2):297–325, 2009.

[27] Seung-Yeal Ha and Eitan Tadmor. From particle to kinetic and hydrodynamic descriptions of flocking. *Kinet. Relat. Models*, 1(3):415–435, 2008.

[28] I.I. Hussein and D.M. Stipanović. Effective coverage control for mobile sensor networks with guaranteed collision avoidance. *IEEE Trans. Control Systems Technology*, 15(4):642–657, 2007.

[29] Joseph LaSalle. Some extensions of liapunov's second method. *IRE Transactions on circuit theory*, 7(4):520–527, 1960.

[30] N.E. Leonard and E. Fiorelli. Virtual Leaders, Artificial Potentials and Coordinated Ccontrol of Groups. *Proc. IEEE Conf. Decision and Control*, 2001.

[31] Zhuchun Li and Xiaoping Xue. Cucker–Smale flocking under rooted leadership with fixed and switching topologies. *SIAM Journal on Applied Mathematics*, 70(8):3156–3174, 2010.

[32] W. Liu, M.B. Short, Y.E. Taima, and A.L. Bertozzi. Multi-scale collaborative searching through swarming. *Proc. Int. Conf. Informatics in Control, Automation, and Robotics*, 2010.

[33] Claudia O López and John E Beasley. A heuristic for the circle packing problem with a variety of containers. *European Journal of Operational Research*, 214(3):512–525, 2011.

[34] Kostas Margellos and John Lygeros. Toward 4-D trajectory management in air traffic control: A study based on monte carlo simulation and reachability analysis. *IEEE Trans. Control Systems Technology*, 21(5):1820–1833, Sep. 2013.

[35] Ian M Mitchell, Alexandre M Bayen, and Claire J Tomlin. A time-dependent Hamilton-Jacobi formulation of reachable sets for continuous dynamic games. *IEEE Transactions on automatic control*, 50(7):947–957, 2005.

[36] R. Olfati-Saber. Flocking for Multi-Agent Dynamic Systems: Algorithms and Theory. *IEEE Trans. Autom. Control*, 51(3):401–421, 2006.

[37] Jaemann Park, H Jin Kim, and Seung-Yeal Ha. Cucker-Smale flocking with inter-particle bonding forces. *IEEE Transactions on Automatic Control*, 55(11):2617–2623, 2010.

[38] W. Ren and Y. Cao. *Distributed Coordination of Multi-agent Networks: Emergent Problems, Models, and Issues*, volume 83 of *Communications and Control Engineering*. Springer-Verlag, London, 2011.

[39] R. Sepulchre, D.A. Paley, and N.E. Leonard. Stabilization of Planar Collective Motion: All-to-All Communication. *IEEE Trans. Automatic Control*, 52(5):1–14, 2007.

[40] Jackie Shen. Cucker–Smale flocking under hierarchical leadership. *SIAM Journal on Applied Mathematics*, 68(3):694–719, 2008.

[41] Qiang Song, Fang Liu, Jinde Cao, and Jianlong Qiu. Cucker-Smale flocking with bounded cohesive and repulsive forces. In *Abstract and Applied Analysis*, volume 2013. Hindawi, 2013.

[42] T. Vicsek, A. Czirók, E. Ben-Jacob, I. Cohen, and O. Shochet. Novel type of phase transition in a system of self-driven particles. *Phys. Rev. Lett.*, 75(6):1226–1229, 1995.

[43] Insoon Yang, Sabine Becker-Weimann, Mina J. Bissell, and Claire J. Tomlin. One-shot computation of reachable sets for differential games. In *Proc. Int. Conf. Hybrid Systems: Computation and Control*, 2013.